論文 / 著書情報
Article / Book Information

題目(和文)	
Title(English)	Periodic Handover Skipping in Cellular Networks and Its Stochastic Geometry Analysis
著者(和文)	徳山喜一
Author(English)	Kiichi Tokuyama
出典(和文)	学位:博士(理学), 学位授与機関:東京工業大学, 報告番号:甲第12655号, 授与年月日:2024年3月26日, 学位の種別:課程博士, 審査員:三好 直人,金森 敬文,髙遠 賢史,中野 張,府川 和彦
Citation(English)	Degree:Doctor (Science), Conferring organization: Tokyo Institute of Technology, Report number:甲第12655号, Conferred date:2024/3/26, Degree Type:Course doctor, Examiner:,,,,
学位種別(和文)	博士論文
Type(English)	Doctoral Thesis

Periodic Handover Skipping in Cellular Networks and Its Stochastic Geometry Analysis

Kiichi Tokuyama

Thesis submitted for
the Degree of Doctor of Science

Department of Mathematical and Comuting Sceience
School of Computing
Tokyo Institute of Technology

2024

Preface

Stochastic geometry is the study of random spatial patterns. Such random structures have been recognized to play a key role in various fields such as cosmology, ecology, cell biology, engineering, and data sciences. One substantial essence in the field of stochastic geometry is the theory of spatial point processes, which are the tools to represent the random allocation of points in a certain given space. The spatial point processes have been applied to various contexts in the real world, for example, random arrivals of customers, distribution of Earthquake location on the whole world.

This thesis studies applications of the stochastic geometry to the handover management problem in wireless cellular communication networks. Handover management has attracted attention of research in the context of wireless cellular communication networks. One crucial problem of handover management is to deal with increasing handovers experienced by mobile users. To address this problem, handover skipping techniques have been studied in recent years. In this thesis, we propose yet another handover skipping scheme, called periodic handover skipping. In the proposed scheme, handovers of a mobile user are controlled by a certain fixed period of time, which we call skipping period. The skipping period can be managed as a system parameter, thereby enabling flexible operation of handover skipping.

We first investigate the periodic handover skipping scheme on a basic model of a single-tier cellular network, where base station in the cellular network are deployed according to a homogeneous Poisson point process. Homogeneous Poisson point processes are often associated with point patterns that do not have any interaction between points. We provide a tractable framework for analyzing the periodic handover skipping scheme. Under a random walk model of user mobility, we derive the analytical expressions of the two performance metrics, the handover rate and the expected downlink data rate. Moreover, by using these two metrics, we construct a utility metric representing transmission performance, regarding the trade-off relation between the handover rate and the data rate. Based on this utility metric, we conduct performance comparison between two scenarios where the periodic

handover skipping scheme is introduced and not introduced.

We next investigate the optimal skipping period on the same single-tier cellular network model, and consider maximizing the utility metric by controlling the skipping period introduced in the periodic handover skipping scheme. Moreover, we attempt to derive an approximate expression of the optimal skipping period. We also conduct numerical comparison with some other handover skipping techniques.

We further study the periodic handover skipping scheme on a two-tier cellular network based on a homogeneous Poisson point process and a Poisson-Poisson cluster process. Poisson-Poisson cluster processes are often used to model clustered nodes in a network, for example, small base stations deployed organically to complement the capacity of the cellular networks at user hotspots. Inside the network, we consider a random walk-based UE with the periodic handover skipping technique. Based on the system model, we provide analytical results for both the handover rate and the expected data rate, which are derived via the exact and the approximate analyses, respectively. In addition, we conduct numerical experiments to verify the efficiency of our proposed model.

Acknowledgements

First of all, I would like to express my gratitude to my supervisor, Professor Naoto Miyoshi, who instructs me in doctor course. He has given me a lot of userful advice and taught me how to write a thesis of research. I would also like to express my gratitude to Professor Toru Ohira, my supervisor in master course. He has taught me ABC of research. Without their support, I could not complete this thesis. I would also like to express my gratitude to the laboratory members. Thanks to them, I had a good time in the laboratory.

I am grateful to Associate Professor Tatsuaki Kimura of Doshisha University. He was Senior Lecturer of Osaka University until an year ago, and gave a lot of valuable advice on how to write a paper by English.

Last but not least, I would like to thank my father for giving me the opportunity to go on to the doctoral course and for keeping to watch over me in every situation. In addition to the people mentioned above, I was able to complete this thesis thanks to the support of many people. I would like to express my deep appreciation here.

Contents

Chapter 1

Introduction

1.1 Basics of stochastic geometry and spatial point processes

Stochastic geometry is the study of random spatial patterns. At the heart of the subject lies the study of random point patterns. Such random structures have been known to play a key role in several branches of natural sciences (cosmology, ecology, cell biology) and engineering (material sciences, networks) for several decades. Their use is currently expanding to new fields like data sciences. One key essence in the field of stochastic geometry is the theory of spatial point processes, which are the tools to represent the random allocation of points in a certain given space. The spatial point processes have been applied to various contexts in the real world, e.g., random arrivals of customers, distribution of Earthquake location on the whole world.

To define the spatial point processes, we first start to define a counting measure. In this thesis, we especially consider the given space as $\mathbb{R}^d$.

Definition 1.1. *A counting measure μ is a locally finite measure on $(\mathbb{R}^d, \mathcal{B}(\mathbb{R}^d))$ such that $\mu(B) \in \mathbb{N}$ for all $B \in \mathcal{B}_c(\mathbb{R}^d)$, where $\mathcal{B}_c(\mathbb{R}^d)$ denotes the set of relatively compact sets in $\mathcal{B}(\mathbb{R}^d)$, i.e., $\mathcal{B}_c(\mathbb{R}^d) := \{B \in \mathcal{B}(\mathbb{R}^d);$ the closure of B is compact$\}$.*

Intuitively, a counting measure μ on $(\mathbb{R}^d, \mathcal{B}(\mathbb{R}^d))$ represents a sample of random allocation of points on the space $\mathbb{R}^d$, since $\mu(B) \in \mathbb{N}$ could represent the number of points included by $B \in \mathcal{B}(\mathbb{R}^d)$ where the pattern of the points is characterized by μ.

Using the above counting measure μ, the point processes on $\mathbb{R}^d$ are defined as follows.

Definition 1.2. *Let* $(\Omega, \mathcal{A}, \mathsf{P})$ *be a probability space,* $\mathbb{M}(\mathbb{R}^d)$ *be the set of counting measures on* $(\mathbb{R}^d, \mathcal{B}(\mathbb{R}^d))$*, and* $\mathcal{M}(\mathbb{R}^d)$ *be the* σ*-algebra on* $\mathbb{M}(\mathbb{R}^d)$ *generated by the mappings* $\mu \to \mu(B)$*. Then, a point process* Φ *is defined as a measurable mapping* $\Phi : \Omega \to \mathbb{M}(\mathbb{R}^d)$*. The probability distribution of* Φ *is* $\mathsf{P}_\Phi = \mathsf{P} \circ \Phi^{-1}$*.*

The point process Φ on $\mathbb{R}^d$ could be considered as a random mapping whose realization is a counting measure. Note that the law of Φ is specified by its probability distribution P_Φ.

1.2 Poisson point process

One important instance of the point process is a Poisson point process (PPP), which is defined as follows.

Definition 1.3. *Let* Λ *be a locally finite measure on* $\mathbb{R}^d$ *and* Φ *be a point process.* Φ *is called PPP with intensity measure* Λ *if for all pairwise disjoint sets* $B_1, \cdots, B_k \in \mathcal{B}(\mathbb{R}^d)$*, the random variables* $\Phi(B_1), \cdots, \Phi(B_k)$ *are independent Poisson random variables with respective means* $\Lambda(B_1), \cdots, \Lambda(B_k)$*; that is, for all* $n_1, \cdots, n_k \in \mathbb{N}$*,*

$$\mathsf{P}(\Phi(B_1) = n_1, \cdots, \Phi(B_k) = n_k) = \prod_{i=1}^{k} \mathrm{e}^{-\Lambda(B_i)} \frac{\Lambda(B_i)^{n_i}}{n_i!}.$$

If the intensity measure Λ is the Lebesgue measure on $\mathbb{R}^d$, then $\Lambda(B_1) = \lambda|B_1|$ for some $\lambda > 0$; that is, the intensity measure is described by the constant λ. In this case, Φ is called a homogeneous PPP of intensity λ.

It is worth noting that a PPP is characterized by the properties described in the following theorem.

Theorem 1.1 ([1, Theorem 2.1.14.])**.** *Let* Φ *be a point process on* $\mathbb{R}^d$ *and satisfy* $\mathsf{P}(\Phi(\{\boldsymbol{x}\}) > 0) = 0$ *for any* $\boldsymbol{x} \in \mathbb{R}^d$*.* Φ *is a PPP if and only if* Φ *has the following properties*

(i) Simplicity; $\mathsf{P}(\Phi(\{\boldsymbol{x}\}) \le 1$ *for all* $\boldsymbol{x} \in \mathbb{R}^d) = 1$*.*

(ii) Complete independence; the random variables $\Phi(B_1), \cdots, \Phi(B_k)$ *are independent for all pairwise disjoint sets* $B_1, \cdots, B_k \in \mathcal{B}(\mathbb{R}^d)$*.*

Due to the above theorem, PPPs are often considered when one does not expect any interactions between points. For example, PPPs on $\mathbb{R}$ are used to model random events distributed in the time axis such as the independent

arrival of customers at a store and the independent occurrence of earthquakes. PPPs on $\mathbb{R}^2$ can represent the locations of scattered objects such as particles colliding into a detector and trees in a forest [2]. Moreover, PPPs are often used to model the locations of wireless nodes in cellular networks, e.g., base stations (BSs) and user equipments (UEs), although there should be some spatial correlations among those nodes [1, 3]. This is because the PPPs are said to be the most analytically tractable among various sorts of point processes due to the independence property [4].

1.3 Poisson-Poisson cluster process

Poisson-Poisson cluster processes (PPCPs) are another instance of point processes that can represent clustering point patterns. A stationary PPCP is made by a parent process and daughter processes, where the parent process represents cluster centers allocated according to a homogeneous PPP, and the daughter processes are independent, identical and finite PPPs located around each point of the parent process. PPCPs are used to model a network if the nodes are clustered, e.g., users gathered around Wi-Fi hot spots [5, 6], and small BSs (SBSs) deployed organically to complement the capacity of the cellular networks at user hotspots or to patch their coverage dead-zones [7].

A PPCP is formally defined as follows.

Definition 1.4. *(i) A PPCP $\Phi(\lambda_p, g, \bar{m})$ on $\mathbb{R}^d$ is*

$$\Phi(\lambda_p, g, \bar{m}) = \bigcup_{z \in \Psi_p} z + C^z, \tag{1.1}$$

where Ψ_p and C^z denote the parent point process and the offspring point process whose cluster center is at $z \in \Psi_p$, respectively. That is, Ψ_p is a homogeneous PPP on $\mathbb{R}^d$ with the intensity λ_p, and $\{q \in C^z\}$ is an independently and identically distributed (i.i.d.) sequence of random vectors with joint probability density function (PDF) $g(q)$. The number of points in C^z is denoted by $M \sim \text{Poisson}(\bar{m})$.

(ii) When the joint PDF g of a PPCP Φ_2 satisfies $g(q) = g_d(\|q\|)$, with a PDF g_d on $\mathbb{R}$, then Φ_2 is called an isotropic PPCP.

A PPCP $\Phi(\lambda_p, g, \bar{m})$ consists of the offspring process C^z shifted by z for each $z \in \Psi_p$, and $x_i \in z + C^z$, $i = 1, \cdots, M$, are conditionally i.i.d with the PDF $g(x_i - z)$.

We next introduce some important properties regarding PPCPs

Proposition 1.1 (Conditional PPP properties of PPCPs [7]). *If a PPCP* $\Phi(\lambda_p, g, \bar{m})$ *is conditioned on the parent point process* Ψ_p*, then* $\Phi(\lambda_p, g, \bar{m})$ *is an inhomogeneous PPP with intensity* $\lambda(\boldsymbol{x}) = \bar{m} \sum_{z \in \Psi_p} g(\boldsymbol{x} - \boldsymbol{z})$.

Proposition 1.1 indicates a PPCP becomes a PPP under the condition that its parent points are fixed. This property could be used to analyze PPCPs since we can apply various analysis results regarding PPPs to PPCPs by giving the condition. The following is the one of the results derived from Proposition 1.1.

Lemma 1.1 (Contact distance distribution [7, Lemma 2]). *If a PPCP* $\Phi(\lambda_p, g, \bar{m})$ *is conditioned on the parent point process* Ψ_p*, then the PDF of the contact distance, i.e., the distance of the nearest point of* $\Phi(\lambda_p, g, \bar{m})$ *from the origin, is given by*

$$f_{cd}(r \mid \Psi_p) = \bar{m} \sum_{z \in \Psi_p} f_d(r \mid \boldsymbol{z}) \prod_{z \in \Psi_p} \mathrm{e}^{-\bar{m} F_d(r|z)}, \tag{1.2}$$

where $f_d(r \mid \boldsymbol{z})$ *denotes the conditional PDF of the distance* $r = \|\boldsymbol{x}\|$ *of an offspring point* $\boldsymbol{x} \in \Phi(\lambda_p, g, \bar{m})$ *from the origin given its cluster center at* $\boldsymbol{z} \in \Psi_p$*, and* $F_d(r \mid \boldsymbol{z})$ *denotes its cumulative distribution function (CDF).*

1.4 Handover management problem in cellular networks

The development of fifth generation (5G) wireless cellular communication systems is driven by the need to satisfy the ever-increasing capacity demand resulting from the proliferation of mobile phones, tablets, and the other handheld mobile devices. One of the key features of the 5G evolution is the network densification through small cell deployment [8]. Densifying base stations (BSs) shrinks the service area of each BS, increases the spectral efficiency, and offers more capacity, thereby enabling a significant increase in the quality of service. However, deploying more BSs promotes frequent handovers (HOs), which increase the risk of disconnection and signaling overhead. Managing and mitigating those frequent HOs is required upon conducting the network densification.

1.4.1 Handover skipping

HO skipping is an approach to address the problem of frequent HOs [9–15], where some HOs of a moving user equipment (UE) are skipped to reduce

excessive HOs. This approach is particularly effective when the UE moves fast, or the network consists of densified small cells. The HO skipping enables a UE to reduce the HO rate, whereas it may decrease the data reception rate (data rate) because it demands the UE to maintain longer connection duration with a BS. Thus, the HO skipping presents a trade-off relation between the increased HO rate and the decreased data rate, and the trade-off relation should be balanced to improve the performance for UEs.

A fundamental HO skipping scheme, which we call *alternate HO skipping*, was introduced in [9]. In this scheme, a UE alternately performs HOs along its trajectory, thereby achieving a 50% reduction in the HO rate. Moreover, they evaluated user throughput analytically for the UEs following the alternate HO skipping schemes. The work [9] was extended in [10] and [11]; [10] introduced the alternate HO skipping in two-tier networks and [11] introduced it in a BS cooperating network with CoMP transmission. Another HO skipping scheme, called *topology-aware HO skipping*, was proposed in [12]. In this scheme, the HO skipping is triggered according to the UE's distance from the target BS and the size of the cell; HOs are not performed when the UE enters a cell whose area is smaller than a certain threshold, or a cell whose dominant BS is farther from the UE than a certain threshold. Thus, the topology-aware HO skipping can prevent the connection distances from being unnecessarily long. The mathematical framework for evaluating topology-aware HO skipping was provided in [13]. They derived the analytical expressions of the coverage probability and the expected data rate when the topology-aware HO skipping is performed under the assumption that the trajectory of a moving UE is a straight line.

1.4.2 Periodic handover skipping

However, both the alternate and the topology-aware HO skippings do not consider the connection duration, i.e., the communication time connecting to a BS until the next HO. Such connection duration is essential for the HO management due to the problem of signaling overhead. More precisely, when a UE performs an HO, its data transmission is temporarily disrupted during the signaling procedure of the HO. This sudden disruption causes unwanted delay and may significantly degrade the performance of network applications. Thus, keeping connection for a certain duration is important for the communication quality of ultra-reliable applications, e.g., high-quality video streaming services and vehicular safety applications. Owing to the above reason, an HO skipping scheme that can control the connection duration should be developed.

We propose yet another HO skipping scheme, called *periodic HO skip-*

ping. Our proposed scheme considers a threshold of time, which we call the *skipping period*, to control frequency of HOs for a moving UE, that is, all HOs attempted earlier than the threshold are skipped, and a UE is guaranteed to keep connected during this threshold time. By adjusting the skipping period, our proposed scheme enables to directly control the connection duration of the UE with a BS.

1.5 Organization of this thesis

This thesis studies the performance analysis and its evaluation of the periodic HO skipping scheme by using spatially stochastic point processes. Chapter 2 investigates the scheme on a basic model of a single-tier cellular network, where BSs are deployed according to a homogeneous PPP. This model is associated with the cellular network model where only one kind of BSs, often called macro BSs (MBSs), are considered. The analytical framework for evaluating the transmission performance is provided in this chapter. Chapter 3 further develops the previous chapter and investigates optimal adjustment of the system parameters introduced in the periodic HO skipping scheme. The investigation in Chapter 4 extends the model of the previous chapter to a two-tier cellular network consisting of MBSs and SBSs, which are allocated according to a homogeneous PPP and a stationary PPCP, respectively. Finally, Chapter 5 concludes the thesis and presents directions for future research. The contents of this thesis have been published as follows. Chapter 2 is based primarily on [16] and [17]. Chapter 3 is based primarily on [17]. Chapter 4 is based primarily on [18].

Chapter 2 proposes the periodic HO skipping scheme and give a study on a single-tier cellular network based on a homogeneous PPP. We investigate the performance of the proposed scheme on the basis of stochastic geometry. Specifically, we derive analytical expressions of two performance metrics– the HO rate and the expected downlink data rate– when a UE adopts the periodic HO skipping. Numerical results based on the analysis demonstrate that the periodic HO skipping scenario can outperform the scenario without any HO skipping in terms of a certain utility metric representing the trade-off between the HO rate and the expected downlink data rate, in particular when the UE moves fast.

Chapter 3 studies the optimal adjustment of the skipping period, the system parameter introduced in the periodic HO skipping scheme proposed in the previous section. Using the analytical results developed in the previous chapter, we numerically evaluate a utility metric representing the transmission performance in the proposed scheme and show that there can exist an

optimal length of the skipping period, which locally maximizes the utility metric, and approximately provide the optimal skipping period in a simple form. Numerical comparison with some other HO skipping techniques is also conducted.

Chapter 4 studies the periodic HO skipping scheme on a two-tier cellular network based on a homogeneous PPP and a stationary PPCP. Inside the network, we consider a random walk-based UE with the periodic HO skipping technique. Based on the system model, we provide analytical results for both the HO rate and the expected data rate, which are derived via the exact and the approximate analyses, respectively. In addition, we conduct numerical experiments to verify the efficiency of our proposed model.

Chapter 2

Data Rate and Handover Rate Analysis of Periodic Handover Skipping in Homogeneous Networks

2.1 Introduction

Theory of spatial point processes and stochastic geometry has become a major tool for performance analysis of wireless communication networks and numerous theoretical/practical results have been developed so far. Among them, many studies have analyzed the data reception rate (data rate for short) for a user equipment (UE) in various settings (see, e.g., [19–21]) as one of the primary performance metrics. However, most of them assume that a UE is fixed at a certain position. On the other hand, there are studies concerning mobility of UEs in the framework of stochastic geometry, which are rather involved in the handover (HO) rate (see, e.g., [22–24]). In terms of data transmission, it would be better for a UE to be associated with a base station (BS) offering higher data rate, which may encourage a mobile UE to have frequent HOs. However, frequent HOs increase the risk of disconnection and signaling overhead. In other words, there is a trade-off between the data rate and the HO rate when a UE is moving.

To address the problem of frequent HOs, an approach of skipping some opportunities of HOs has been considered, which is called HO skipping (see, e.g., [9–15]). While various HO skipping techniques have so far been proposed and studied in such a point of view, we propose yet another HO skipping scheme, called *periodic HO skipping*. The proposed scheme prohibits the HOs

of a mobile UE for a certain period of time, referred to as *skipping period*, thereby enabling flexible operation of the HO skipping by adjusting the length of the skipping period. In this chapter, we investigate the performance of the proposed scheme from the perspective of the trade-off between the HO rate and the data rate.

2.1.1 Related work

A number of studies have so far analyzed the performance of cellular networks with mobile UEs and many of them have adopted stochastic geometry as an analytical tool (see, e.g., recent tutorial articles [34, 35] and references therein). In the stochastic geometry approach, the locations of wireless nodes (BSs and/or UEs) in a wireless network are modeled by stochastic point processes on the Euclidean plane, so that we can capture the spatial irregularity of wireless nodes and explore mathematical analysis of region-independent network performance by virtue of the theory of point processes and stochastic geometry. The first results along this line date back to the late 1990s [22, 36], where the cells associated with BSs in a cellular network are modeled as the Voronoi tessellation formed by a homogeneous Poisson point process (PPP) and some performance metrics concerning mobile UEs are discussed. Since the 2010s, this stream has become more active. Lin *et al.* [23] propose a mobility model of a UE on single-tier hexagonal/PPP networks and analyze the HO rate and the expected sojourn time of a mobile UE staying in a particular cell. The results in [23] are then extended in [37] to a two-tier heterogeneous network (HetNet). Bao and Liang [24] derive an analytical expression for the HO rate in a multi-tier HetNet modeled using overlaid independent PPPs and provide a guideline for tier selection taking both the HO rate and the expected downlink data rate into account. In addition, [29] develops a similar analysis to [24] for a single-tier network with BS cooperation. Sadr and Adve [31] analyze the HO rate in a PPP model of multi-tier HetNets with orthogonal spectrum allocation among tiers and investigate the negative impact of HOs on the coverage probability. Chattopadhyay *et al.* [30] evaluate the expected downlink data rate for a mobile UE taking into account the data outage periods due to HOs in a two-tier HetNet and further discuss the fraction of connecting BSs to reduce frequent HOs.

Several HO skipping techniques have also been proposed and analyzed using the stochastic geometry (see, e.g., [9–13]). Arshad *et al.* [9] introduce the so-called alternate HO skipping, where a mobile UE executes HOs alternately along its trajectory, and quantify the average throughput representing the trade-off between the HO rate and the expected downlink data rate when a UE adopts the alternate HO skipping. The results in [9] are extended in [10]

to a two-tier HetNet and in [11] to the incorporation with BS cooperation. Furthermore, [12] proposes topologyaware HO skipping, where a UE skips an HO when the target BS is far from the UE's trajectory or the cell of the target BS is small, and evaluates its performance by Monte Carlo simulations. Demarchou *et al.* [13] then provide a mathematical analysis of the topology-aware HO skipping. Compared with these sophisticated HO skipping techniques, our proposed scheme is simple and easy to implement since it is enough for a mobile UE to observe the BS locations every fixed-length period (as seen in the definition of the scheme in Sec. 2.2.2).

2.1.2 Contributions

The contributions of this work are summarized as follows.

1) We propose and advocate the periodic HO skipping, which prohibits the HOs of a mobile UE during each cycle of the skipping period.

2) Applying the stochastic geometry approach, we derive the analytical expressions of the HO rate and the expected downlink data rate when a mobile UE adopts the periodic HO skipping.

3) On the basis of the analytical results, we numerically demonstrate that the proposed scheme can outperform the conventional scenario without any HO skipping, in particular when the UE moves fast.

2.1.3 Organization

The rest of this chapter is organized as follows. In the next section, we describe the network model and our proposed periodic HO skipping scheme. We then define the user mobility model and the performance metrics; that is, the expected downlink data rate and the HO rate. In Sec. 2.3, the performance of the proposed scheme is investigated, where for comparison, we analyze the performance metrics not only for the proposed scheme but also for the scenario without any HO skipping. Then, on the basis of the analytical results, the performances of the two scenarios are numerically compared in terms of a certain utility metric representing the trade-off between the data rate and the HO rate. Finally, this chapter is concluded in Sec. 2.5.

2.2 System model

2.2.1 Network model

In this chapter, we develop our proposed periodic HO skipping scheme implemented on the most basic spatially stochastic model of cellular networks; that is, a homogeneous PPP network with Rayleigh fading and power-law path-loss (see, e.g., [19, 38]). Before defining the proposed scheme, we detail here the network model.

BSs in a cellular network are deployed according to a homogeneous PPP $\Phi = \sum_{i\in\mathbb{N}} \delta_{X_i}$ on the Euclidean plane $\mathbb{R}^2$ with intensity $\lambda \in (0,\infty)$, where $\mathbb{N} := \{1, 2, \cdots\}$, $\delta_{\boldsymbol{x}}$ denotes the Dirac measure with mass at $\boldsymbol{x} \in \mathbb{R}^2$, and the points $X_1, X_2, \cdots$ of Φ are numbered in an arbitrary order. All the BSs transmit signals with the same power level, normalized to one, using a common spectrum bandwidth. We suppose that the time is divided into discrete slots and the downlink channels are affected by Rayleigh fading and power-law path-loss. Moreover, we assume that shadowing effects are averaged out and normalized to one. The reason is that the time variation is little compared to the fading effects, and this assumption promotes tractability in our analysis. Therefore, if a UE located at $\boldsymbol{u} \in \mathbb{R}^2$ at slot $t \in \mathbb{N}_0 := \mathbb{N} \cup \{0\}$ receives a signal from the BS at X_i, $i \in \mathbb{N}$, the received signal power is represented by $H_{i,t}\|X_i - \boldsymbol{u}\|^{-\beta}$, where $\|\cdot\|$ stands for the Euclidean norm, $H_{i,t}$, $i \in \mathbb{N}, t \in \mathbb{N}_0$, are mutually independent and exponentially distributed random variables with unit mean representing the fading effects, and $\beta > 2$ denotes the path-loss exponent.

We assume that, at any time slot, each BS has at least one UE in service and transmits a signal to one of its UEs. Then, if a UE is located at $\boldsymbol{u} \in \mathbb{R}^2$ at slot $t \in \mathbb{N}_0$ and is served by the BS at X_i, the downlink signal-to-interference-plus-noise ratio (SINR) for this UE is represented by

$$\mathsf{SINR}_{\boldsymbol{u},i}(t) = \frac{H_{i,t}\|X_i - \boldsymbol{u}\|^{-\beta}}{I_{\boldsymbol{u},i}(t) + \sigma^2}, \quad i \in \mathbb{N},\ t \in \mathbb{N}_0, \tag{2.1}$$

where σ^2 denotes a nonnegative constant representing the noise power and $I_{\boldsymbol{u},i}(t)$ denotes the total interference power to this UE given by

$$I_{\boldsymbol{u},i}(t) = \sum_{j\in\mathbb{N}\setminus\{i\}} H_{j,t}\|X_i - \boldsymbol{u}\|^{-\beta}. \tag{2.2}$$

The instantaneous downlink data rate $\xi_{\boldsymbol{u},i}(t)$ is then defined as

$$\xi_{\boldsymbol{u},i}(t) = \log(1 + \mathsf{SINR}_{\boldsymbol{u},i}(t)), \tag{2.3}$$

where log stands for the natural logarithm for simplicity, but of course, it can be converted into the conventional binary logarithm by multiplying the constant $\log_2 \mathrm{e}$. Note that Shannon's channel capacity is particularly considered in the definition of the data rate. We further note that narrow bandwidth is mainly supposed for the utilized channel. The reason is that frequency-selective fading effects are mitigated in the narrow-band channel and therefore the channel capacity is likely to be achievable compared to the broadband channel.

2.2.2 Periodic handover skipping

Suppose that a UE moves on $\mathbb{R}^2$ and is initially (at slot 0) served by its nearest BS, which offers the strongest signal power to the UE when the fading effects are averaged out. In other words, the cells of respective BSs form a Poisson-Voronoi tessellation (see [2, Sec. 9.7]). In our proposed periodic HO skipping scheme, a UE is prohibited from executing HOs and retains the initial connection for s time slots, referred to as *skipping period*, regardless of its motion. After the skipping period of s slots has passed, the UE reexamines the connection and if the current connection is no longer with the nearest BS due to its moving, the UE executes an HO and makes a new connection with the nearest one. Afterward, this procedure is repeated in cycles of the skipping period. Namely, the UE reexamines its connection to a BS every s time slots, during which it skips any chances of HOs even if it crosses the boundaries between cells. We assume that an HO, if it is done, is executed instantly without any time loss. We should note that a UE is always connected to its nearest BS at the beginning of each cycle of the skipping period, whereas it does not always execute an HO at the end of a cycle since the current connection can still be with the nearest one.

One may claim that the skipping period described above is similar to the time-to-trigger (TTT) in Long-Term Evolution (LTE) [39]. Indeed, they both suppress the number of HOs by prohibiting them for a certain period of time. However, they are substantially different in that the TTT starts at the instant that a UE crosses a boundary between two cells and it is in the order of 100msec, which mainly aims to prevent ping-pong phenomena around the boundaries between cells. On the other hand, the skipping period repeats in cycles and prohibits HOs during each cycle, which is in the order of seconds (though it may depend on the speed of the UE).

Clearly, the choice of the length of the skipping period is vital for our proposed scheme. If the skipping period is too short, it results in frequent HOs, whereas the long skipping period may cause long-distance connections, which deteriorate the transmission performance. Therefore, we should decide

the length of the skipping period carefully.

2.2.3 Mobility model

Owing to the spatial stationarity of the network model, we can focus on a UE that is supposed to be at the origin $\mathbf{0} = (0, 0) \in \mathbb{R}^2$ at slot 0 and we refer to this UE as the *typical UE*. Let $S(t)$ denote the location of the typical UE at slot $t \in \mathbb{N}_0$. Since a UE is allowed to execute an HO every cycle of the skipping period in our proposed scheme, it is enough to observe the location of the typical UE every cycle and we model its motion as a simple and tractable random walk on $\mathbb{R}^2$. Let $Y_1, Y_2, \cdots$ denote a sequence of independent and identically distributed (i.i.d.) random variables on $\mathbb{R}^2$ representing the motions of the typical UE in respective cycles of the skipping period. Then, the location of the typical UE just after n cycles (that is, at slot ns) is provided as a random work;

$$S(ns) = \sum_{k=1}^{n} Y_k, \quad n \in \mathbb{N}, \tag{2.4}$$

with $S(0) = \mathbf{0}$. We assume that the typical UE moves along the straight line segment at a constant velocity during each cycle; that is, $\{S(t)\}_{t\in\mathbb{N}_0}$ is piecewise deterministic and is given by

$$S(t) = S(ns) + \frac{t - ns}{s} Y_{n+1}, \quad t = ns, ns + 1, \cdots, (n + 1)s, \; n \in \mathbb{N}_0. \tag{2.5}$$

An example of a path of the typical UE is illustrated in Fig. 2.1. Let $Y_n = (L_n, \psi_n)$, $n \in \mathbb{N}$, in the polar coordinates. Then, the moving speed of the typical UE during the nth cycle is equal to $V_n = L_n/s$. It is reasonable to suppose that the moving distance L_n in a cycle depends on the cycle length s; that is, L_n is stochastically larger as s is larger. Hence, we provide the distribution of V_n, instead of L_n, and that of ψ_n for our mobility model and assume that these distributions do not depend on the cycle length. The distributions of V_n and ψ_n respectively represent changes in speed and direction of the typical UE over cycles of the skipping period, and the choice of these distributions gives enough flexibility to our model to capture various mobility patterns. For instance, $\mathsf{P}(V_n = 0) > 0$ represents that the UE can take a pause for s time slots with a positive probability, and if ψ_n takes a constant, the UE always moves along a straight line.

2.2.4 Performance metrics

As discussed in Sec. 2.1, the HO skipping induces the trade-off between the HO rate and the data rate. We thus evaluate the performance of our proposed

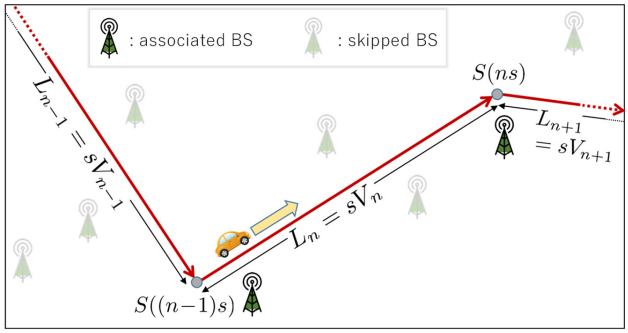

Figure 2.1: A path of the typical UE in the random walk mobility model.

scheme in terms of the expected downlink data rate $\mathcal{T}$ and the HO rate $\mathcal{H}$, which are respectively defined as

$$\mathcal{T} = \lim_{m\to\infty} \frac{1}{m} \mathbb{E}\left[\sum_{t=0}^{m-1} \xi(t)\right], \tag{2.6}$$

$$\mathcal{H} = \lim_{m\to\infty} \frac{\mathbb{E}[\zeta(0,m)]}{m}, \tag{2.7}$$

where $\xi(t)$ denotes the instantaneous downlink data rate for the typical UE at slot t, specifically given in (2.3), and $\zeta(a,b)$ denotes the number of HOs executed by the typical UE from slot a to slot b. These performance metrics are analyzed and evaluated in the following sections.

2.3 Performance analysis and evaluation

In this section, we investigate the performance of our proposed scheme introduced in the preceding section. For comparison, we analyze the performance metrics defined in (2.6) and (2.7) not only in the scenario with the proposed periodic HO skipping but also in the conventional scenario without any HO skipping on the same network and mobility models described in Secs.2.2.1 and 2.2.3. In the scenario without HO skipping, the typical UE certainly executes an HO whenever it crosses a boundary between two cells. We refer to the scenario without HO skipping and that with the periodic HO skipping as Scenario 0 and Scenario 1, respectively, and distinguish elements in the respective scenarios by putting the superscript "(0)" or "(1)"; for example, $\mathcal{T}^{(0)}$ and $\mathcal{H}^{(0)}$ respectively stand for the expected downlink data rate and the HO rate in Scenario 0, whereas $\mathcal{T}^{(1)}$ and $\mathcal{H}^{(1)}$ are those in Scenario 1.

2.3.1 Expected downlink data rate analysis

Expected Downlink Data Rate in Scenario 0

In Scenario 0, the typical UE certainly executes an HO whenever it crosses a boundary between two cells; that is, the typical UE is always connected to its nearest BS. The following proposition is directly derived from the existing result in the literature.

Proposition 2.1. *For the cellular network model described in Sec. 2.2, the expected downlink data rate in Scenario 0 is given by*

$$\mathcal{T}^{(0)} = \int_0^\infty \int_0^\infty \frac{\rho(z,w)}{1+z}\,\mathrm{d}z\,\mathrm{d}w, \tag{2.8}$$

where

$$\rho(z,w) = \exp\left(-\sigma^2 z\left(\frac{w}{\pi\lambda}\right)^{\beta/2} - w\left(1+\frac{2z^{2/\beta}}{\beta}\int_{1/z}^\infty \frac{v^{2/\beta-1}}{1+v}\,\mathrm{d}v\right)\right),$$

Proof. For $\boldsymbol{u} \in \mathbb{R}^2$, let $B(\boldsymbol{u})$ denote the index of the nearest point of $\Phi = \sum_{i\in\mathbb{N}} \delta_{X_i}$ to the location $\boldsymbol{u}$; that is, $\left\|X_{B(\boldsymbol{u})} - \boldsymbol{u}\right\| < \|X_i - \boldsymbol{u}\|$ for $i \in \mathbb{N}\backslash\{B(\boldsymbol{u})\}$. Suppose that the typical UE is located at $S(t) = \boldsymbol{u}$ at slot $t \in \mathbb{N}_0$. Since $\sum_{i=1}^\infty \delta_{X_i - \boldsymbol{u}}$ is equal in distribution to Φ due to the stationarity and $H_{i,t}, i \in \mathbb{N}, t \in \mathbb{N}_0$, are i.i.d., we have from (2.1) with (2.2) that $\mathrm{SINR}_{u,B(u)}(t)$ is equal in distribution to $\mathrm{SINR}_{\mathbf{0},B(\mathbf{0})}(0)$ for any $\boldsymbol{u} \in \mathbb{R}^2$. Thus, since $\{S(t)\}_{t\in\mathbb{N}_0}$ is independent of Φ and $\left\{H_{i,t}\right\}_{i\in\mathbb{N},t\in\mathbb{N}_0}$, the definition of the expected downlink data rate in (2.6) leads to

$$\begin{aligned}\mathcal{T}^{(0)} &= \lim_{m\to\infty}\frac{1}{m}\sum_{t=0}^{m-1}\mathbb{E}\left[\xi_{S(t),B(S(t))}(t)\right]\\ &= \mathbb{E}\left[\boldsymbol{\xi}_{\mathbf{0},B(\mathbf{0})}(0)\right],\end{aligned}$$

which implies that the expected downlink data rate in Scenario 0 is equal to that for a static UE. Hence, the existing result of the expected downlink data rate for a static UE gives (2.8) (see, e.g., [19, Theorem 3]). □

Remark 2.1. *Proposition 2.1 implies that, if a moving UE is always connected to its nearest BS, the expected downlink data rate is identical to that for a static UE. Note that this fact is derived under the condition that Φ is stationary, $H_{i,t}, i \in \mathbb{N}, t \in \mathbb{N}_0$, are i.i.d., and $\{S(t)\}_{t\in\mathbb{N}_0}$ is independent of Φ and $\left\{H_{i,t}\right\}_{i\in\mathbb{N},t\in\mathbb{N}_0}$. In other words, this holds true even when the locations of BSs are according to a general stationary point process and the fading effects independently follow a general identical distribution. A similar discussion is found in [30, Remark 2].*

Expected Downlink Data Rate in Scenario 1

In Scenario 1, the typical UE is not always connected to its nearest BS but remains connected to the BS that is the nearest at the beginning of each cycle of the skipping period.

Theorem 2.1. *For the cellular network model described in Sec. 2.2, the expected downlink data rate in Scenario 1 with s slots of the skipping period is given by*

$$\mathcal{T}^{(1)} = \frac{1}{s}\sum_{t=0}^{s-1}\int_0^\infty \tau(tv)\mathrm{d}F_V(v), \tag{2.9}$$

where F_V denotes the distribution function of the moving speed $V_1 = \|Y_1\|/s$ of the typical UE in a cycle of s slots and

$$\tau(u) = \int_0^\infty \frac{1}{z}\exp\left(-\sigma^2 z - \pi\lambda K_\beta z^{2/\beta}\right)(\mu(z,u)-1)\mathrm{d}z, \tag{2.10}$$

with

$$K_\beta = \frac{2\pi}{\beta}\csc\frac{2\pi}{\beta}, \tag{2.11}$$

$$\mu(z,u) = 2\pi\lambda\int_0^\infty r\exp\left(-\lambda\left[\pi r^2 - J(r,z,u)\right]\right)\mathrm{d}r, \tag{2.12}$$

$$J(r,z,u) = 2z\int_0^\pi\int_0^r \frac{x}{z + w_{x,u,\phi}^\beta}\mathrm{d}x\ \mathrm{d}\phi, \tag{2.13}$$

and $w_{x,u,\phi} = \sqrt{x^2+u^2-2xu\cos\phi}$.

The proof of Theorem 2.1 relies on the following lemma.

Lemma 2.1. *Suppose that a UE is located at $\boldsymbol{u}\in\mathbb{R}^2$ with $\|\boldsymbol{u}\| = u$ at slot $t\in\{0,1,\ldots,s-1\}$ and is served by the BS at $X_{B(\mathbf{0})}$, which is the nearest BS to the origin. Then, the expected instantaneous downlink data rate for this UE satisfies $\mathbb{E}\left[\xi_{\boldsymbol{u},B(\mathbf{0})}(t)\right] = \tau(u)$ given in* (2.10).

Proof. See Section 2.4.1. □

Proof of Theorem 2.1. As in the proof of Proposition 2.1, let $\boldsymbol{B}(\boldsymbol{u})$ denote the index of the nearest point of $\Phi = \sum_{i\in\mathbb{N}}\delta_{X_i}$ to $\boldsymbol{u}\in\mathbb{R}^2$. In Scenario 1, we see from (2.4) and (2.5) that the typical UE is connected to the BS at

$X_{B(S(ns))}$ at slot $ns+t$ for $n \in \mathbb{N}_0$ and $t \in \{0, 1, \ldots, s-1\}$. Thus, the expected downlink data rate in (2.6) is reduced to

$$\begin{aligned}\mathcal{T}^{(1)} &= \lim_{m\to\infty} \frac{1}{m} \sum_{n=0}^{\lfloor m/s \rfloor} \sum_{t=0}^{s-1} \mathbb{E}\left[\xi_{S(ns+t),B(S(ns))}(ns+t)\right] \\ &= \frac{1}{s} \sum_{t=0}^{s-1} \mathbb{E}\left[\xi_{S(t),B(\mathbf{0})}(t)\right], \end{aligned} \tag{2.14}$$

where the last equality follows from the distributional equivalence among $\mathrm{SINR}_{S(ns+t),B(S(ns))}(ns+t)$ and $\mathrm{SINR}_{S(t),B(\mathbf{0})}(t)$ for $t \in \{0, 1, \ldots, s-1\}$, which follows because Φ is stationary and isotropic, $H_{i,t}, i \in \mathbb{N}, t \in \mathbb{N}_0$, are i.i.d., and also $Y_k, k \in \mathbb{N}$, in (2.4) are i.i.d. and independent of Φ and $\left\{H_{i,t}\right\}_{i\in\mathbb{N},t\in\mathbb{N}_0}$. Hence, we obtain (2.9) since $\mathbb{E}\left[\xi_{S(t),B(\mathbf{0})}(t) \mid S(t) = \boldsymbol{u}\right] = \tau(tv)$ when $\|\boldsymbol{u}\| = tv$ by Lemma 2.1 and $\|S(t)\| = (t/s)\|Y_1\| = tV_1$ for $t \in \{0, 1, \ldots, s-1\}$ by (2.5). □

The expressions from (2.9) to (2.13) obtained in Theorem 2.1 are indeed numerically computable. However, they include some nested integrals, which may annoy us with a heavy computational load. In the rest of this subsection, we discuss some ways of reducing the computational load.

Tips for Computational Load Reduction

We here introduce some tips to reduce the load of computing $\mathcal{T}^{(1)}$ in Theorem 2.1 exactly or approximately. First, we find that a simple change of variables reduces the number of nested integrals.

Lemma 2.2. *Function J in* (2.13) *is equal to the following.*

$$J(r, z, u) = 2z \int_0^{u+r} \frac{x}{z + x^\beta} C(x, r, u)\mathrm{d}x, \tag{2.15}$$

with

$$C(x, r, u) = \begin{cases} \pi, & u = 0, \\ \arccos\left(-1 \vee \frac{x^2+u^2-r^2}{2xu} \wedge 1\right), & u > 0, \end{cases}$$

where $a \vee b = \max\{a, b\}$ and $a \wedge b = \min\{a, b\}$ for $a, b \in \mathbb{R}$.

Proof. See Section 2.4.2. □

We can observe through experiments that (2.15) reduces the computation time of the expected instantaneous downlink data rate $\tau(u)$ by about 60%

u(km)	0.1	0.2	0.3	0.4	0.5	0.6
Use of eq. (2.13) (sec)	1344	973	10221	7286	4754	1474
Use of eq. (2.15) (sec)	695	1118	1196	632	974	401

Table 2.1: Comparison of the computation time of $\tau(u)$ using (2.13) and (2.15). The paramenter values are fixed at $\lambda = 10$ (units/km^2), $\beta = 3$ and $\sigma^2 = 25$.

on average compared to the use of (2.13) (see Table 2.1). Next, we give a simple lower bound for τ in (2.10) under the interference-limited (noise-free) assumption.

Corollary 2.1. *Suppose that $\sigma^2 = 0$. Then, τ in* (2.10) *is bounded below as follows.*

$$\tau(u) \geq \frac{\beta}{2} \int_0^\infty \frac{z^{\beta/2-1}}{(1+z)\left(K_\beta^{\beta/2} + z^{\beta/2}\right)} \exp\left(-\pi\lambda u^2 \frac{z}{1+z}\right) \mathrm{d}z, \quad u \geq 0, \tag{2.16}$$

with K_β given in (2.11).

Proof. See Section 2.4.3. □

Remark 2.2. *As we can see in the proof, the lower bound in Corollary 2.1 is obtained by relaxing the condition that there must not be other BSs closer than the nearest BS to the origin. Similar bounds/approximates are often found in the literature (see, e.g., [40]).*

The lower bound obtained in Corollary 2.1 is indeed of a simple form (including a single integral), but as seen in Fig. 2.2, it causes non-negligible gaps from the exact values, in particular when the moving distance u is small, whereas the gaps decrease as u increases. On the other hand, we know that $\tau(0) = \mathcal{T}^{(0)}$ since the expected downlink data rate in Scenario 0 is equal to that for a static UE. Hence, we can approximate τ in (2.10) by interpolating between $\mathcal{T}^{(0)}$ and the lower bound in Corollary 2.1 as follows. Suppose $\sigma^2 = 0$ as in Corollary 2.1 and let $\widetilde{\tau}$ denote the lower bound of τ given on the right-hand side of (2.16). Then, τ in (2.10) is approximated as

$$\tau(u) \approx \epsilon(u)\mathcal{T}^{(0)} + (1 - \epsilon(u))\widetilde{\tau}(u), \quad u \geq 0, \tag{2.17}$$

where a function $\epsilon : [0, \infty) \to [0, 1]$ is smooth and decreasing, and satisfies $\epsilon(0) = 1$ and $\epsilon(u) \to 0$ as $u \to \infty$; that is, it is chosen in such a way that the right-hand side of (2.17) is close to $\mathcal{T}^{(0)}$ when u is small, and it approaches

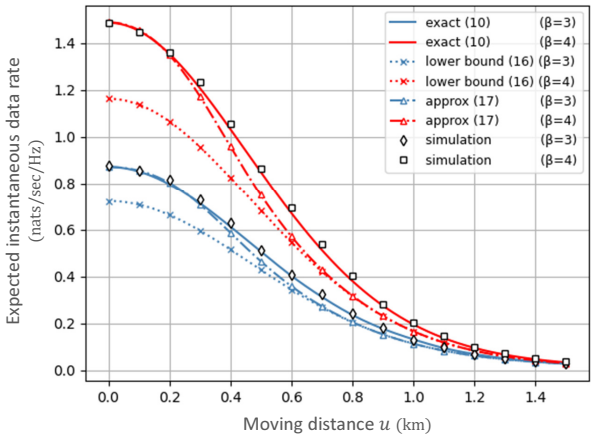

Figure 2.2: Numerical comparison of τ in (2.10) with the lower bound (2.16), the approximation (2.17), and the values from Monte Carlo simulation. The BS intensity is fixed at $\lambda = 1$ (units/km^2) and two patterns of $\beta = 3$ and $\beta = 4$ are exhibited.

$\widetilde{\tau}(u)$ as u becomes larger. Figure 2.2 compares the numerical results of τ in (2.10) with its lower bound in (2.16) and the approximation in (2.17), as well as with the values from Monte Carlo simulation, with respect to the moving distance u. In the approximation (2.17), the function ϵ is set as $\epsilon(u) = e^{-10u^2}, u \geq 0$. The simulation results are computed as the mean of 10,000 independent samples. As stated above, the values of the lower bound have some gaps from the exact values when u is small, whereas these gaps decrease as u increases. This implies that the condition that other BSs never exist closer than the nearest BS is nonnegligible when the typical UE is close to the origin, but it is diminishing as the UE moves away from the origin. On the other hand, the approximation (2.17) shows good agreement with the exact values as expected. However, we should note that such agreement depends on a choice of the function ϵ. An exponential function $\epsilon(u) = e^{-au^b}$ as above seems an plausible choice as one with the desired properties (that is, smooth and decreasing with $\epsilon(0) = 1$ and $\lim_{u\to\infty} \epsilon(u) = 0$), and statistical fitting of a and b would lead to better results.

2.3.2 Handover rate analysis

We now proceed to the analysis of the HO rate. Similar to the proof of Theorem 2.1, the HO rate in (2.7) is reduced to

$$\begin{aligned}\mathcal{H} &= \lim_{m\to\infty} \frac{1}{m} \sum_{n=0}^{\lfloor m/s \rfloor} \mathbb{E}[\zeta(ns,(n+1)s)] \\ &= \frac{\mathbb{E}[\zeta(0,s)]}{s},\end{aligned} \tag{2.18}$$

where the last equality follows since $\mathbf{\Phi}$ is stationary and isotropic, and $Y_k, k \in \mathbb{N}$, in (2.4) are i.i.d. and independent of $\mathbf{\Phi}$. By (2.18), it is enough to consider the expected number of HOs in a cycle of s slots, during which the typical UE moves along a straight line segment, and we can use the existing results in both Scenarios 0 and 1.

HO Rate in Scenario 0

The HO rate in the scenario without any HO skipping has so far been studied in the literature. The following is a direct consequence of it.

Proposition 2.2. *For the cellular network model described in Sec. 2.2, the HO rate in Scenario 0 is given by*

$$\mathcal{H}^{(0)} = \frac{4\sqrt{\lambda}\bar{v}}{\pi}, \tag{2.19}$$

where $\bar{v}$ denotes the average moving speed of the typical UE in a cycle of s slots; that is, $\bar{v} = \mathbb{E}[V_1]$ with $V_1 = \|Y_1\|/s$.

Proof. Given $L_1 = \|Y_1\| = \ell$, the conditionally expected number of HOs $\mathbb{E}\left[\zeta^{(0)}(0,s) \mid L_1 = \ell\right]$ in a cycle is equal to the expected number of intersections of a line segment of length ℓ with the boundaries of the Poisson-Voronoi cells, and is well-known as $\mathbb{E}\left[\zeta^{(0)}(0,s) \mid L_1 = \ell\right] = 4\sqrt{\lambda}\ell/\pi$ (see, e.g., [23, 41, 42]). Applying this to (2.18) with $L_1 = sV_1$ derives (2.19) by taking the expectation. □

HO Rate in Scenario 1

The HO rate in a similar scenario to our Scenario 1 is studied in [31], which helps us to show the following.

Proposition 2.3. *For the cellular network model described in Sec. 2.2, the HO rate in Scenario 1 with s slots of the skipping period is given by*

$$\mathcal{H}^{(1)} = \frac{1}{s}\left[1 - 2\lambda \int_0^\infty \int_0^\pi \int_0^\infty r e^{-\lambda\eta(r,sv,\phi)} \mathrm{d}r \ \mathrm{d}\phi \mathrm{d}F_V(v)\right], \tag{2.20}$$

where

$$\eta(r,\ell,\phi) = w_{r,\ell,\phi}^2 \arccos\left(\frac{r\cos\phi - \ell}{w_{r,\ell,\phi}}\right) + r^2(\pi - \phi) + r\ell\sin\phi, \tag{2.21}$$

with $w_{r,\ell,\phi} = \sqrt{r^2 + \ell^2 - 2r\ell\cos\phi}$, and F_V is (as in (2.9)) the distribution function of the moving speed $V_1 = \|Y_1\|/s$ of the typical UE in a cycle of s slots.

Proof. By the isotropy of $\Phi = \sum_{i\in\mathbb{N}} \delta_{X_i}$, we can assume without loss of generality that the typical UE moves in the positive direction along the horizontal axis during a cycle of s slots. Suppose that the typical UE initially connected to the BS at $X_{B(\mathbf{0})} = \boldsymbol{x} = (r,\phi)$ in the polar coordinates and moves to $Y_1 = \boldsymbol{y} = (\ell, 0)$ in s slots. Let $b_{\boldsymbol{x}}(r)$ denote the disk centered at $\boldsymbol{x} \in \mathbb{R}^2$ with radius $r > 0$. Since there are no BSs in $b_{\mathbf{0}}(r)$ and the distance to the initial BS at $\boldsymbol{x}$ from the location y is equal to $w_{r,\ell,\phi} = \sqrt{r^2 + \ell^2 - 2r\ell\cos\phi}$, the typical UE executes an HO at the end of the cycle if and only if there is at least one BS in the area $b_y\left(w_{r,\ell,\phi}\right) \setminus b_0(r)$. Hence, similar discussion to [31] gives

$$\begin{aligned}
&\mathbb{E}\left[\zeta^{(1)}(0,s) \mid X_{B(\mathbf{0})} = (r,\phi), Y_1 = (\ell,0)\right] \\
&= 1 - e^{-\lambda\left|b_y\left(w_{r,\ell,\phi}\right)\setminus b_0(r)\right|} \\
&= 1 - \exp\left(-\lambda\left[w_{r,\ell,\phi}^2 \arccos\left(\frac{r\cos\phi - \ell}{w_{r,\ell,\phi}}\right) - r^2\phi + r\ell\sin\phi\right]\right),
\end{aligned} \tag{2.22}$$

where $|A|$ denotes the Lebesgue measure of $A \in \mathcal{B}\left(\mathbb{R}^2\right)$. This can be unconditioned by integrating with respect to the density $f_0(r)\mathrm{d}r = 2\pi\lambda r e^{-\pi\lambda r^2}\ \mathrm{d}r$ of $\left\|X_{B(\mathbf{0})}\right\|$ over $[0,\infty)$, $\mathrm{d}\phi/\pi$ over $[0,\pi)$, and $\mathrm{d}F_V(v)$ over $[0,\infty)$ with $v = \ell/s$. Finally, plugging it into (2.18), we have (2.20). □

2.3.3 Numerical evaluation of performance metrics

We here numerically evaluate the expected downlink data rate and the HO rate in the periodic HO skipping scheme, which are respectively obtained in Theorem 2.1 (with Lemma 2.2) and Proposition 2.3. Throughout the

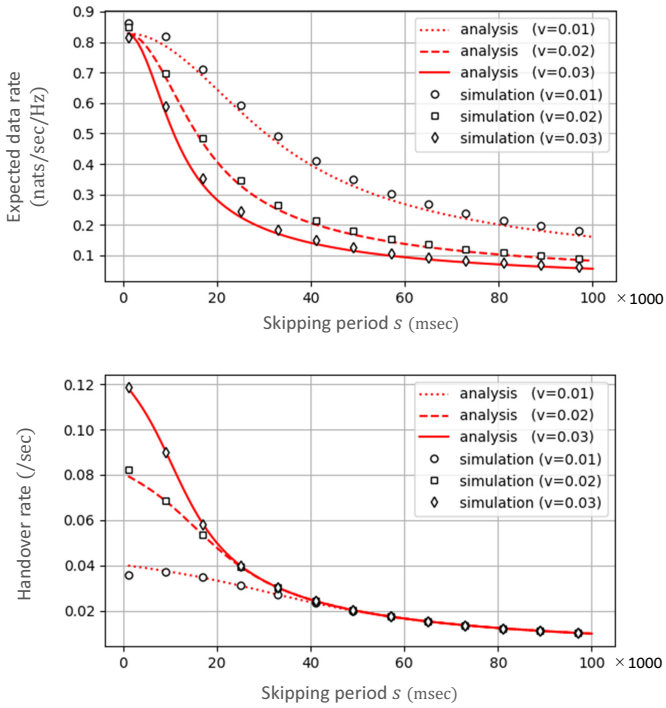

Figure 2.3: The performance metrics as functions of the length s of the skipping period for three patterns of the moving speed $v = 0.01, 0.02$, and 0.03 (km/sec).

experiments, we set as 1slot = 1msec, the intensity of the BSs, the path-loss exponent, and the noise power are fixed at $\lambda = 10$ (units /km^2), $\beta = 3$, and $\sigma^2 = 25$, respectively, and the moving speed $V_1 = \|L_1\|/s$ of the typical UE is given as a constant. Figure 2.3 shows the curves of $\mathcal{T}^{(1)}$ and $\mathcal{H}^{(1)}$ with respect to the length s of the skipping period. For comparison, the values from Monte Carlo simulation are also plotted as the means of 1,000 independent samples of $\sum_{t=0}^{m-1} \xi^{(1)}(t)/m$ and $\zeta^{(1)}(0,m)/m$, respectively with $m = 1000$ (cf. (2.6) and (2.7)). We find that the analytical results match well with the simulation results. Moreover, we can confirm the trade-off relation between the HO rate and the expected downlink data rate; that is, both are decreasing in the length of the skipping period. We further explore this trade-off in the next subsection.

2.3.4 Utility metric

To discuss the trade-off between the expected downlink data rate $\mathcal{T}$ and the HO rate $\mathcal{H}$, we introduce a utility metric $\mathcal{U}$ as

$$\mathcal{U} = \mathcal{T} - c\mathcal{H}, \tag{2.23}$$

where a utility constant $c > 0$ is suitably chosen so as to convert the negative impact of HOs into the loss of the downlink data rate. Note that similar metrics are found in the literature (cf. [10, 24, 29, 35]) and are often referred to as the user throughput accounting for the loss due to HOs. However, we do not use the term "throughput" in this chapter because $\mathcal{U}$ in (2.23) can take negative values (see, e.g., Fig. 2.4 below).

Figure 2.4 compares the utility metrics $\mathcal{U}^{(0)}$ and $\mathcal{U}^{(1)}$ respectively for Scenarios 0 and 1 with respect to the average speed $\bar{v} = \mathbb{E}[V_1]$ of the typical UE. In the computation of $\mathcal{U}^{(1)}$, τ in (2.9) is replaced by its approximation (2.17) with the adjustment function $\epsilon(u) = e^{-10u^2}$. Four different distributions of the moving speed are experimented with the common average $\bar{v}$; that is, exponential, second-order Erlang, second-order hyper-exponential, and deterministic ones, where in the hyper-exponential distribution, two exponential distributions with means $\bar{v}/2$ and $3\bar{v}/2$ are mixed with equal probability. The other parameters are fixed as $\lambda = 1$ (units /km^2), $\beta = 3$, $\sigma^2 = 0, s = 50,000$(msec), and $c = 10$ (nats/Hz). Note that only one line is exhibited for $\mathcal{U}^{(0)}$ since it depends on the distribution of the moving speed only through its average (as confirmed from (2.8) and (2.19)). From Fig. 2.4, we observe that Scenario 0 shows better performance when the average moving speed is small (roughly $\bar{v} \leq 0.05$(km/sec)), whereas Scenario 1 becomes better as the UE moves faster. This is thought to be because $\mathcal{H}^{(0)}$ is linearly increasing in $\bar{v}$ (see (2.19)), whereas $\tau(u)$ in (2.10) is slowly decreasing in u (see Fig. 2.2). Moreover, we find an interesting property from the experiment that the distribution of the moving speed has an impact on the utility metric in Scenario 1; that is, the utility metric takes larger values as the distribution of the moving speed is larger in variation. Exploration of this property will be left for future work.

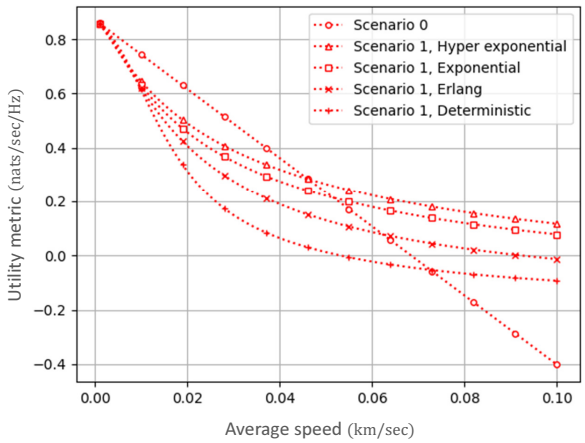

Figure 2.4: The values of $\mathcal{U}^{(0)}$ and $\mathcal{U}^{(1)}$ as functions of the average speed $\bar{v}$ of the moving UE with several distributions.

2.4 Proofs of Lemmas and Corollary

2.4.1 Proof of Lemma 2.1

Applying Hamdi's Lemma [43, Lemma 1] to the expectation of (2.3) with (2.1), (2.2) and $i = B(\mathbf{0})$, we have

$$\begin{aligned}\mathbb{E}\left[\xi_{\boldsymbol{u},B(\mathbf{0})}(t)\right] &= \mathbb{E}\left[\log\left(1+\frac{H_{B(\mathbf{0}),t}\left\|X_{B(\mathbf{0})}-\boldsymbol{u}\right\|^{-\beta}}{I_{\boldsymbol{u},B(\mathbf{0})}(t)+\sigma^2}\right)\right] \\ &= \int_0^\infty \frac{e^{-\sigma^2 z}}{z}\left(\mathbb{E}\left[e^{-zI_{\boldsymbol{u},\boldsymbol{B}(\mathbf{0})}(t)}\right]-\mathbb{E}\left[e^{-z\sum_{j\in\mathbb{N}}H_{j,t}\left\|X_j-\boldsymbol{u}\right\|^{-\beta}}\right]\right)\mathrm{d}z,\end{aligned} \tag{2.24}$$

For the second expectation in the last expression above, the Laplace transform of an exponential distribution and the generating functional of a PPP (e.g., [44, Example 9.4(c)]) yield

$$\begin{aligned}\mathbb{E}\left[\prod_{j\in\mathbb{N}} e^{-zH_{j,t}\left\|X_j-\boldsymbol{u}\right\|^{-\beta}}\right] &= \mathbb{E}\left[\prod_{j\in\mathbb{N}}\left(1+\frac{z}{\left\|X_j-\boldsymbol{u}\right\|^{\beta}}\right)^{-1}\right] \\ &= \exp\left(-\lambda z\int_{\mathbb{R}^2}\frac{1}{z+\|\boldsymbol{x}\|^{\beta}}\mathrm{d}\boldsymbol{x}\right) \\ &= e^{-\pi\lambda K_\beta z^{2/\beta}},\end{aligned} \tag{2.25}$$

with $K_\beta = (2\pi/\beta)\csc(2\pi/\beta)$ as given in (2.11), where we use the polar coordinate conversion and $\int_0^\infty w^{a-1}/(1+w)\mathrm{d}w = \pi\csc a\pi$ for $a \in (0,1)$ in the

last equality. Next, we consider the first expectation in the last expression of (2.24), which satisfies

$$\mathbb{E}\left[e^{-zI_{\boldsymbol{u},B(\mathbf{0})}(t)}\right] = \int_0^\infty \mathbb{E}\left[e^{-zI_{\boldsymbol{u},B(\mathbf{0})}(t)} \mid \left\|X_{B(\mathbf{0})}\right\| = r\right] f_0(r)\mathrm{d}r, \tag{2.26}$$

where $f_0(r) = 2\pi\lambda r e^{-\pi\lambda r^2}$ gives the probability density function of $\left\|X_{B(\mathbf{0})}\right\|$. Similar to obtaining (2.25), we have

$$\begin{aligned}
&\mathbb{E}\left[e^{-zI_{\boldsymbol{u},B(\mathbf{0})}(t)} \mid \left\|X_{B(\mathbf{0})}\right\| = r\right] \\
&= \mathbb{E}\left[\prod_{j\in\mathbb{N}\setminus\{B(\mathbf{0})\}} \left(1 + \frac{z}{\left\|X_j - \boldsymbol{u}\right\|^\beta}\right)^{-1} \mid \left\|X_{B(\mathbf{0})}\right\| = r\right] \\
&= \exp\left(-\lambda z \int_{\|\boldsymbol{x}\|>r} \frac{1}{z + \|\boldsymbol{x} - \boldsymbol{u}\|^\beta}\mathrm{d}\boldsymbol{x}\right) \\
&= \exp\left(-\pi\lambda K_\beta z^{2/\beta} + \lambda z \int_{\|\boldsymbol{x}\|\le r} \frac{1}{z + \|\boldsymbol{x} - \boldsymbol{u}\|^\beta}\mathrm{d}\boldsymbol{x}\right),
\end{aligned} \tag{2.27}$$

where the polar coordinate conversion gives

$$z\int_{\|x\|\le r} \frac{1}{z + \|\boldsymbol{x} - \boldsymbol{u}\|^\beta}\mathrm{d}\boldsymbol{x} = J(r, z, u), \tag{2.28}$$

with J given in (2.13). Plugging (2.27) together with (2.28) into (2.26), we have

$$\mathbb{E}\left[e^{-zI_{\boldsymbol{u},B(\mathbf{0})}(t)}\right] = e^{-\pi\lambda K_\beta z^{2/\beta}}\mu(z, u), \tag{2.29}$$

with μ in (2.12). Finally, plugging (2.25) and (2.29) into (2.24) derives (2.10).

2.4.2 Proof of Lemma 2.2

It is immediate for the case of $u = 0$ since $w_{x,0,\phi} = x$ in (2.13). Suppose $u > 0$. On the left-hand side of (2.28), changing the variables as $\boldsymbol{x}' = \boldsymbol{u} - \boldsymbol{x}$ leads to

$$\int_{\|\boldsymbol{x}\|\le r} \frac{1}{z + \|\boldsymbol{x} - \boldsymbol{u}\|^\beta}\mathrm{d}\boldsymbol{x} = \int_{b_{\boldsymbol{u}}(r)} \frac{1}{z + \|\boldsymbol{x}'\|^\beta}\mathrm{d}\boldsymbol{x}',$$

where $b_{\boldsymbol{u}}(r)$ denotes the disk centered at $\boldsymbol{u} \in \mathbb{R}^2$ with radius $r > 0$. Recall that $\|\boldsymbol{u}\| = u$ as in Lemma 2.1. When $u \ge r$, the polar coordinate conversion

gives (see Fig. 2.5a)

$$\begin{aligned}
&\int_{b_{\boldsymbol{u}}(r)} \frac{1}{z+\|\boldsymbol{x}\|^{\beta}} \mathrm{d}\boldsymbol{x} \\
&= 2\int_{u-r}^{u+r} \frac{x}{z+x^{\beta}} \arccos\left(\frac{x^2+u^2-r^2}{2xu}\right) \mathrm{d}x \\
&= 2\int_{0}^{u+r} \frac{x}{z+x^{\beta}} \arccos\left(\frac{x^2+u^2-r^2}{2xu} \wedge 1\right) \mathrm{d}x, \qquad (2.30)
\end{aligned}$$

where the last equality holds since $f(x) = \left(x^2+u^2-r^2\right)/(2xu) > 1$ for $x \in (0, u-r)$ with $f(u-r) = 1$ when $u \geq r > 0$. On the other hand, when $u < r$, we have similarly (see Fig. 2.5b),

$$\begin{aligned}
&\int_{b_{u}(r)} \frac{1}{z+\|\boldsymbol{x}\|^{\beta}} \mathrm{d}\boldsymbol{x} \\
&= 2\pi\int_{0}^{r-u} \frac{x}{z+x^{\beta}} \mathrm{d}x + 2\int_{r-u}^{u+r} \frac{x}{z+x^{\beta}} \arccos\left(\frac{x^2+u^2-r^2}{2xu}\right) \mathrm{d}x \\
&= 2\int_{0}^{u+r} \frac{x}{z+x^{\beta}} \arccos\left(-1 \vee \frac{x^2+u^2-r^2}{2xu}\right) \mathrm{d}x, \qquad (2.31)
\end{aligned}$$

where the last equality holds since $f(x) = \left(x^2+u^2-r^2\right)/(2xu) < -1$ for $x \in (0, r-u)$ with $f(r-u) = -1$ when $0 < u < r$. Hence, unifying (2.30) and (2.31), we have (2.15) since $\left(x^2+u^2-r^2\right)/(2xu) \in [-1, 1]$ when $|u-r| \leq x \leq u+r$.

2.4.3 Proof of Corollary 2.1

In (2.24) with $\sigma^2 = 0$, changing the variables as $z' = \left\|X_{B(0)} - \boldsymbol{u}\right\|^{-\beta} z$ leads to

$$\begin{aligned}
&\mathbb{E}\left[\xi_{\boldsymbol{u},B(\boldsymbol{0})}(t)\right] \\
&= \int_{0}^{\infty} \frac{1}{z'} \mathbb{E}\left[e^{-\|X_{B(\boldsymbol{0})}-\boldsymbol{u}\|^{\beta} z' I_{\boldsymbol{u},\boldsymbol{B}(\boldsymbol{0})}(t)} \left(1 - e^{-z' \boldsymbol{H}_{\boldsymbol{B}(\boldsymbol{0}),t}}\right)\right] \mathrm{d}z' \\
&= \int_{0}^{\infty} \frac{1}{1+z} \mathbb{E}\left[e^{-\|X_{\boldsymbol{B}(\boldsymbol{0})}-\boldsymbol{u}\|^{\beta} z \boldsymbol{I}_{\boldsymbol{u},\boldsymbol{B}(\boldsymbol{0})}(t)}\right] \mathrm{d}z, \qquad (2.32)
\end{aligned}$$

where the second equality follows from $\mathbb{E}\left[e^{-zH_{B(\boldsymbol{0}),t}} \mid B(\boldsymbol{0})\right] = (1+z)^{-1}$ because $H_{i,t}, i \in \mathbb{N}$, $t \in \mathbb{N}_0$, are mutually independent and exponentially distributed with unit mean. Furthermore, since $\left\|X_{B(\boldsymbol{0})}\right\|$ follows the probability density function $f_0(r) = 2\pi\lambda r e^{-\pi\lambda r^2}$ and the angle between $X_{B(\boldsymbol{0})}$ and $\boldsymbol{u}$ is uniformly

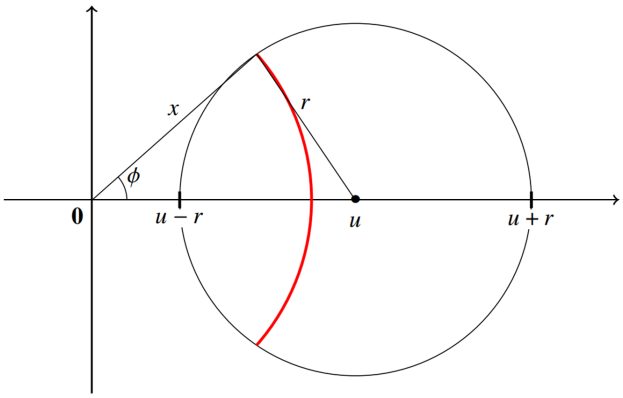

(a) Case of $u \geq r$, where x varies from $u - r$ to $u + r$.

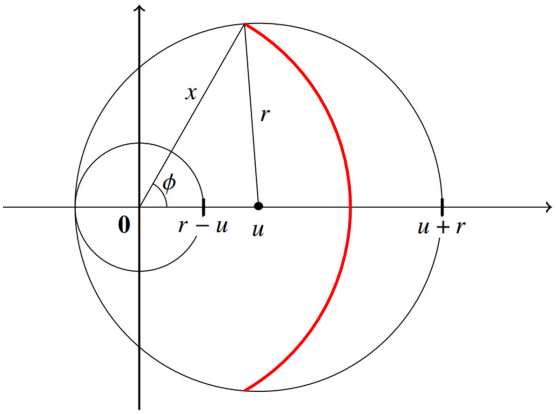

(b) Case of $u < r$, where x varies from $r - u$ to $u + r$.

Figure 2.5: Supplement to the derivation of eqs. (2.30) and (2.31), where $\phi = \arccos\left(\frac{x^2+u^2-r^2}{2xu}\right)$ for each $x \in [|u-r|, u+r]$.

distributed on $[0, 2\pi)$, the expectation in the last expression of (2.32) satisfies

$$
\begin{aligned}
&\mathbb{E}\left[e^{-\|X_{B(\mathbf{0})}-\boldsymbol{u}\|^{\beta} z I_{\boldsymbol{u},B(\mathbf{0})}(t)}\right] \\
&= \frac{1}{2\pi}\int_0^{2\pi}\int_0^{\infty} \mathbb{E}\left[e^{-w_{r,u,\phi}{}^{\beta} z I_{\boldsymbol{u},B(\mathbf{0})}(t)} \mid \left\|X_{B(\mathbf{0})}\right\| = r\right] f_0(r)\mathrm{d}r\ \mathrm{d}\phi \\
&\geq \lambda\int_0^{2\pi}\int_0^{\infty} r\exp\left(-\pi\lambda r^2 - \pi\lambda K_\beta w_{r,u,\phi}{}^2 z^{2/\beta}\right)\mathrm{d}r\ \mathrm{d}\phi \\
&= \lambda e^{-\pi\lambda K_\beta u^2 z^{2/\beta}}\int_0^{2\pi}\int_0^{\infty} r\exp\left(-\pi\lambda\left[\left(1+K_\beta z^{2/\beta}\right)r^2 - 2K_\beta u z^{2/\beta} r\cos\phi\right]\right)\mathrm{d}r\ \mathrm{d}\phi \\
&= \frac{1}{1+K_\beta z^{2/\beta}}\exp\left(-\pi\lambda u^2\frac{K_\beta z^{2/\beta}}{1+K_\beta z^{2/\beta}}\right),
\end{aligned}
\tag{2.33}
$$

where $w_{r,u,\phi} = \sqrt{r^2 + u^2 - 2ru\cos\phi}$ and the inequality follows from (2.27), from which the nonnegative integral term is removed. In the last equality in (2.33), we apply the following; that is, for $p > 0$ and $q \in \mathbb{R}$,

$$\begin{aligned}\int_0^{2\pi}\int_0^{\infty} re^{-pr^2+qr\cos\phi}\mathrm{d}r\ \mathrm{d}\phi &= \int_{-\infty}^{\infty}\int_{-\infty}^{\infty} e^{-p\left(x^2+y^2\right)+qx}\ \mathrm{d}x\ \mathrm{d}y \\ &= e^{q^2/(4p)}\int_{-\infty}^{\infty}\int_{-\infty}^{\infty} e^{-p\left(x^2+y^2\right)}\mathrm{d}x\ \mathrm{d}y \\ &= \frac{\pi}{p}e^{q^2/(4p)}.\end{aligned}$$

Finally, plugging (2.33) into (2.32) and changing the variables as $z' = K_\beta z^{2/\beta}$, we obtain (2.16).

2.5 Conclusion

In this chapter, we have proposed a simple HO skipping scheme in cellular networks, called the periodic HO skipping, and have evaluated its performance analytically and numerically. Specifically, applying the stochastic geometry approach, we have derived numerically computable expressions for the expected downlink data rate and the HO rate when the UE adopts the proposed scheme. Through the numerical experiments based on the analysis, we have confirmed that the proposed scheme can outperform the scenario without any HO skipping in terms of a utility metric representing the trade-off between the expected downlink data rate and the HO rate, in particular when the UE moves fast.

Chapter 3

Optimal Skipping Period

3.1 Introduction

The development of the fifth generation mobile communication systems (5G) is driven by the ever-increasing demand for channel capacity due to the proliferation of mobile user equipments (UEs) such as mobile phones, tablets, and other handheld devices. One of the key solutions in the 5G evolution is network densification through small cell deployments (see, e.g., [32, 33]). Densifying base stations (BSs) offers more capacity, which improves the quality of service. On the other hand, it shrinks the service area of each BS and induces frequent handovers (HOs), which may increase the signaling overhead and the risk of disconnections.

HO skipping is an approach to address the problem of frequent HOs by skipping some opportunities of HOs (see, e.g., [9–15]). However, in turn, the HO skipping may decrease the data reception rate (data rate for short) since it tends to force a UE to retain long-distance connection with a BS. In other words, the HO skipping induces a trade-off between the HO rate and the data rate, and this trade-off should be balanced for the network densification to work effectively.

3.1.1 Related work

To investigate the impact of HOs on transmission performance of UEs in cellular networks, a number of studies have focused on analyzing the trade-off relation between the HO rate and the data rate. For their theoretical analysis, the theory of spatial point processes and stochastic geometry have been adopted to model cellular networks (see, e.g., [34, 35] for surveys). In the stochastic geometry approach, the deployment of nodes is modeled by a stochastic point process, which can capture its randomness in the real

world. Moreover, applying the stochastic geometry approach enables us to obtain rigorous mathematical expressions of performance metrics as a function depending on various system parameters; thereby, we can grasp how the system parameters are generally involved in those performance metrics through the expressions. For example, the trade-off relation between the HO rate and the data rate are analyzed for heterogeneous cellular networks (HetNets) in [24] and for a BS cooperated cellular network with coordinated multi-point (CoMP) transmission in [29]. Maximizing user throughput in a two-tier network is considered in [30], where they found the optimal proportion of macro and small BSs density and their respective transmit power levels by balancing the HO rate and the data rate for multiple static and moving UEs. Some related work considered a trade-off relation between the HO rate and the coverage probability; the work [31] considered the HO rate in multi-tier HetNets and analyzed the negative effect of performing HOs on the coverage probability. Using the analysis results, they derived the optimal proportion of the BSs density in different tiers to maximize the coverage probability of a typical UE.

The HO skipping is a user-centric approach for mitigating the effect of frequent HOs [9–15]. This approach aims to balance the trade-off relation between the HO rate and the data rate by controlling the frequency of HOs directly for the UEs. In [9], an *alternate HO skipping* scheme is studied, where a UE alternately performs HOs along its trajectory, thereby achieving a 50% reduction in the HO rate. Considering the trade-off relation, they evaluated user throughput analytically for the UEs following the alternate HO skipping schemes. The work [9] was extended in [10] and [11]; [10] introduced the alternate HO skipping in two-tier networks and [11] introduced it in a BS cooperating network with CoMP transmission. In [13], a *topology-aware HO skipping* scheme is studied with its mathematical framework. In this scheme, the HO skipping is triggered according to the UE's distance from the target BS and the size of the cell. They derived the analytical expressions of the coverage probability and the expected data rate when the topology-aware HO skipping is performed under the assumption that the trajectory of a moving UE is a straight line. In [16], a *periodic HO skipping* scheme is studied. They consider to control HOs of a mobile UE by a certain fixed period of time, called skipping period, and analyze the HO rate and the expected data rate for the UE following the periodic HO skipping scheme. Moreover, they found the periodic HO skipping scheme could outperform the conventional non-HO skipping scenario by comparing a utility metric representing the trade-off between the HO rate and the data rate.

3.1.2 Contribution

This work enhances [16], where the periodic HO skipping is already proposed, and considers maximization of the utility metric defined in [16] by adjusting the skipping period of the periodic HO skipping scheme. Moreover we will find later that, with the optimal adjustment of the skipping period, the periodic HO skipping scheme can compete with the other sophisticated HO skipping schemes such as ones in [9] and [13]. The contributions of this work are summarized as follows.

1) We numerically observe that there can exist an optimal length of the skipping period and provide an approximate optimal skipping period in a simple computable form.

2) We numerically observe that the proposed scheme can compete with some other sophisticated HO skipping techniques.

3.1.3 Organization

The rest of this chapter is organized as follows. Section 3.2 is the preliminaries regarding the utility metric and the results of analysis used in the following sections. In Sec. 3.3, we discuss how to decide the length of the skipping period, where we numerically observe that there exists an optimal length of the skipping period which locally maximizes the utility metric. We then provide a simple computable expression of an approximate optimal skipping period. Some properties of the approximate optimal skipping period are also revealed by numerical experiments. Numerical comparison with some other HO skipping techniques are made in Sec. 3.5. Finally, this chapter is concluded in Section 3.7.

3.2 Preliminaries

Since we consider the same models regarding the network, the periodic HO skipping scheme, and the mobility of UEs, we here omit that description (see Sec. 2.2 for the system model). We here describe again the definition of the utility metric and the results of analysis given in the previous chapter, which are used in the following discussion of this chapter.

3.2.1 Utility metric

Let $\mathcal{T}$ and $\mathcal{H}$ denote the expected downlink data rate and the HO rate of the typical UE in the scenario where the typical UE attempts the periodic

HO skipping scheme described in the previous chapter (see Sec. 2.2.2). Here, $\mathcal{T}$ and $\mathcal{H}$ are defined as follows

$$\mathcal{T} = \lim_{m\to\infty} \frac{1}{m} \mathsf{E}\left[\sum_{t=0}^{m-1} \xi(t)\right], \quad \mathcal{H} = \lim_{m\to\infty} \frac{1}{m} \mathsf{E}\big[\zeta(m)\big], \tag{3.1}$$

where $\xi(t)$ denotes the data rate at the time $t \in \mathbb{N}_0$, which is given in (2.3), and $\zeta(m)$ denotes the number of experienced HOs from the time 0 to m of the typical UE in the scenario of the periodic HO skipping. Using the above two metrics, the utility metric is defined as follows [24, 29]

$$\mathcal{U} = \mathcal{T} - c\mathcal{H}, \tag{3.2}$$

where $c > 0$ is the cost for an HO[1].

The intuitive background behind the definition in (3.2) is to indicate the trade-off relation between the expected data rate and the HO rate, that is, the utility of data reception penalized by the cost of performing an HO. A related performance evaluation function, called the mobility-aware throughput, is described in [35], where they considered the trade-off relation between the HO rate and the data rate to indicate the throughput of a moving UE.

3.2.2 Results of analysis

Theorem 3.1 (Theorem 2.1 and Lemma 2.2)**.** *The expected data rate $\mathcal{T}$ in the periodic HO skipping scenario is*

$$\mathcal{T} = \frac{1}{s} \sum_{t=0}^{s-1} \mathsf{E}[\tau(tV_1)], \tag{3.3}$$

where V_1 is the moving speed of the typical UE described in Sec. 2.2.3, and $\tau(u)$, $u \geq 0$, is given by

$$\tau(u) = \lambda \int_0^{2\pi}\int_0^{\infty}\int_0^{\infty} r\, \mathrm{e}^{-\pi\lambda r^2 - \sigma^2 w_{u,r,\theta}^{\beta} z}\, \frac{\rho(z, r, \theta|u)}{1+z}\, \mathrm{d}z\mathrm{d}r\mathrm{d}\theta, \tag{3.4}$$

where

$$\rho(z, r, \theta|u) = \exp\left(-2\pi\lambda \left\{ w_{u,r,\theta}^2 K_\beta\, z^{\frac{2}{\beta}} - \int_0^{u+r} \widetilde{\varphi}_{u,r,x} \left\{1 + \frac{1}{z}\Big(\frac{x}{w_{u,r,\theta}}\Big)^{\beta}\right\}^{-1} x\mathrm{d}x \right\}\right),$$

[1] As described in Section 3.1, performing HOs has several negative impacts, such as the disconnection and the signaling overhead. In our model, such negative impacts of HOs are regarded as transformed to the amount of lost data by the constant c.

with

$$K_\beta = \frac{\pi}{\beta} \csc \frac{2\pi}{\beta}, \tag{3.5}$$

$$\widetilde{\varphi}_{u,r,x} = \pi^{-1} \cos^{-1}\Big(-1 \vee \frac{u^2 - r^2 + x^2}{2ux} \wedge 1\Big), \tag{3.6}$$

$$w_{u,r,\theta} = \sqrt{u^2 + r^2 - 2ur\cos\theta}. \tag{3.7}$$

Corollary 3.1 (Corollary 2.1)**.** *If $\sigma^2 = 0$, that is, noise power is negligible, then the expected data rate $\mathcal{T}$ in the periodic HO skipping scenario is given in* (3.3)*, where the lower bound of $\tau(u)$, $u \geq 0$, is given by*

$$\tau(u) \geq \tau'(u) = \int_0^\infty \frac{\beta/2}{1 + (K_\beta z^{-1})^{\beta/2}} \cdot \frac{\exp\left(-\frac{2\pi\lambda z}{1+2z} u^2\right)}{1+2z} z^{-1} dz, \tag{3.8}$$

with K_β which is given in (3.5)*.*

Corollary 3.2 (eq.(2.17))**.** *If $\sigma^2 = 0$, then the expected data rate $\mathcal{T}$ in the periodic HO skipping scenario is given in* (3.3)*, where $\tau(u)$ is approximately given by*

$$\tau(u) \approx \tau''(u, \varepsilon) = \mathrm{e}^{-\varepsilon u^2} \mathcal{T}_0 + (1 - \mathrm{e}^{-\varepsilon u^2}) \tau'(u), \tag{3.9}$$

where $\mathcal{T}_0$ is given by

$$\mathcal{T}_0 = \int_0^\infty \int_0^\infty \frac{\rho_0(z, w)}{1+z} \, \mathrm{d}z \, \mathrm{d}w, \tag{3.10}$$

with

$$\rho_0(z, w) = \exp\left\{-\sigma^2 z \left(\frac{w}{\pi\lambda}\right)^{\beta/2} - w\left(1 + \frac{2z^{2/\beta}}{\beta} \int_{1/z}^\infty \frac{v^{2/\beta - 1}}{1+v} \, \mathrm{d}v\right)\right\}.$$

and $\tau'(u)$ are given in (3.10) *and* (3.8)*, respectively. Moreover, $\varepsilon > 0$ is a fitting parameter.*

Proposition 3.1 (Proposition 2.3)**.** *The HO rate $\mathcal{H}$ in the periodic HO skipping scenario is given as*

$$\mathcal{H} = \frac{1}{s} \mathsf{E}[\eta(sV_1)], \tag{3.11}$$

where $\eta(l)$, $l > 0$, is given by

$$\eta(l) = 1 - 2\lambda \int_0^\pi \int_0^\infty r \mathrm{e}^{-\lambda\{\pi r^2 + \varrho(r,\theta|l)\}} \mathrm{d}r \mathrm{d}\theta, \tag{3.12}$$

with

$$\varrho(r, \theta|l) = {w_{l,r,\theta}}^2 \Big[\theta + \sin^{-1}\left(\frac{l \sin\theta}{w_{l,r,\theta}}\right)\Big] - r^2\theta + lr\sin\theta, \tag{3.13}$$

and $w_{l,r,\theta}$ is given in (3.7)*.*

3.3 Analysis of optimal skipping period

In this section, we consider to maximize the utility metric with respect to the skipping period. First, we evaluate the utility metric $\mathcal{U}$ given in (3.2) using some approximations. Next, we analyze the optimal skipping period that maximizes the approximated utility metric.

3.3.1 Approximation of utility metric

We assume that the moving speed of the typical UE is conditioned on $V_1 = v > 0$. Then, by combining (3.3) and (3.11) with (3.2), the utility metric is given by

$$\mathcal{U}(s) = \frac{1}{s}\sum_{t=0}^{s-1}\tau(tv) - \frac{c}{s}\eta(sv), \tag{3.14}$$

where $\tau(tv)$ and $\eta(sv)$ are given in (3.4) and (3.12), respectively. Although the parameter s in the function above is a positive integer, we modify the function to make s continuous; we regard the sum on the right-hand side of (3.14) as a Riemann sum and approximate it by the corresponding integral, that is

$$\sum_{t=0}^{s-1}\tau(tv) \approx \frac{1}{v}\int_0^{sv}\tau(u)\,\mathrm{d}u.$$

In addition, we replace $\tau(u)$ with $\tau'(u)$ in (3.8) for the sake of simplicity. We then obtain an approximate continuous function of $\mathcal{U}$(s) as follows:

$$\mathcal{U}(s) \approx \widetilde{\mathcal{U}}(s) := \frac{1}{v}\int_0^{v}\tau'(sw)\mathrm{d}w - \frac{c}{s}\eta(sv). \tag{3.15}$$

3.3.2 Analytical expression of optimal skipping period

We here consider to maximize the above utility metric $\widetilde{\mathcal{U}}$(s). In fact, $\widetilde{\mathcal{U}}$(s) is expected to have a local maximum especially when the moving speed v is sufficiently small. We refer to the length s of the skipping period which gives the local maximum of the utility metric as the *optimal skipping period*. Here we show this fact with the approximate expression of the optimal skipping period.

Theorem 3.2. *For the cellular network model described in Sec. 2.2, we suppose that the typical UE adopts the periodic HO skipping and moves at certain*

constant speed v. Then, an approximation of the optimal skipping period is obtained as the closest integer of s^* given by

$$s^* \approx \frac{15-\pi^2}{4\pi^2\beta} c \Big(\int_0^\infty \frac{1}{1+(K_\beta z^{-1})^{\beta/2}} \cdot \frac{1}{(1+2z)^2} \mathrm{d}z \Big)^{-1}, \tag{3.16}$$

where K_β is given in (3.5).

Proof. See Section 3.6. □

Remark 3.1. *Although this expression is obtained under the condition that v is sufficiently small, numerical studies suggest that it is applicable to general cases of the moving speed v: see the discussion in Sec. 3.4.1.*

3.4 Numerical evaluation

3.4.1 Accuracy of approximate utility metric

We first examine the approximation error of $\widetilde{\mathcal{U}}(\mathrm{s})$ in (3.15) compared with $\mathcal{U}(s)$ in (3.14) in terms of their optimal skipping period. Fig. 3.1 shows the numerical results of the utility metrics. From the figure, we see that both the two utility metrics have similar shapes, although there are some errors between them. In particular, both the metrics exhibit a local maximum. In addition, the values of the optimal skipping period for the two metrics are observed to be similar. Also, the optimal skipping period is almost invariant with respect to v. Furthermore, since $\mathcal{U}(\mathrm{s})$ and $\widetilde{\mathcal{U}}(\mathrm{s})$ converge to zero as s increases, we expect that when v is sufficiently small, the local maximum indicates the maximum uniquely at least on a finite value range of a practical setting. Since both the exact and approximate utility metrics have similar optimal skipping period, we conclude that the approximate utility metric $\widetilde{\mathcal{U}}(\mathrm{s})$ has enough accuracy for evaluating the optimal skipping period.

3.4.2 Numerical evaluation of s^*

We here numerically evaluate s^* obtained in Theorem 3.2. Figure 3.2 shows the numerical results of s^* (the time unit = msec) with respect to the path-loss exponent β and the utility constant c. The BS intensity and the moving speed of the typical UE are fixed as $\lambda = 1$ (units /km^2) and $v = 0.01$(km/sec), respectively. For comparison, the values of s, which locally maximize the approximate utility metric $\widetilde{\mathcal{U}}(\mathrm{s})$ in (3.15), are numerically searched and plotted in the figure. From Fig. 3.2, we observe that the values of s^* agree well with

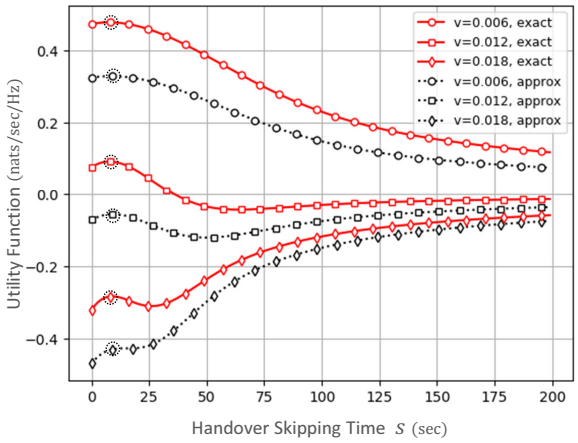

Figure 3.1: Numerical samples of $\mathcal{U}(\mathrm{s})$ and $\widetilde{\mathcal{U}}(\mathrm{s})$, which are plotted in the red solid lines and the black dotted lines, respectively. Three patterns of the values of the moving speed v are exhibited where $v = 0.006, 0.012, 0.018$ (km/sec), and the other system parameters are fixed as $\lambda = 3$ (units/km^2), $c = 30$ (nats/Hz), $\sigma^2 = 0$, and $\beta = 3$.

the values from the numerical search even for positive moving speed, in particular for large β and small c, in spite that s^* is derived under the condition of sufficiently small moving speed. Figure 3.2a shows that s^* is decreasing in β. This is thought to be because $\tau'(u)$ decays more rapidly with respect to u when β is larger (as confirmed in Fig. 2.2); that is, smaller s brings better performance when β is larger since $\widetilde{\mathcal{U}}(\mathrm{s})$ has the term $\frac{1}{v}\int_0^v \tau'(sw)\mathrm{d}w$. On the other hand, Fig. 3.2b shows that s^* is linearly increasing in c (as is clear from (3.16)). This is interpreted as because $\widetilde{\mathcal{U}}(\mathrm{s})$ is linearly decreasing in c, and thus better performance is given by larger s which makes the HO rate lower.

Figure 3.3 further compares the values of s^* in (3.16) and the numerically searched values of s as above with respect to the constant moving speed v of the typical UE. Since s^* does not depend on v and λ (see (3.16)), its value is given as a horizontal line for each pair of β and c. Note that the values of the optimal skipping period obtained by the numerical search do not change significantly with respect to the changes in v and λ, in particular for large β and small c, which allows us to use s^* in (3.16) as an approximation of the optimal skipping period for any v and λ, in particular when β is large and c is small.

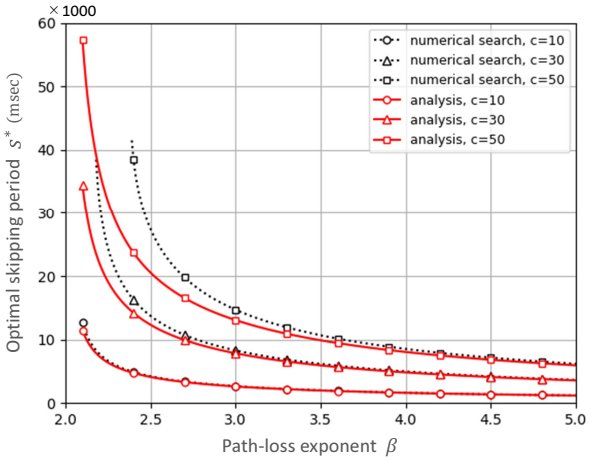

(a) s^* as a function of β.

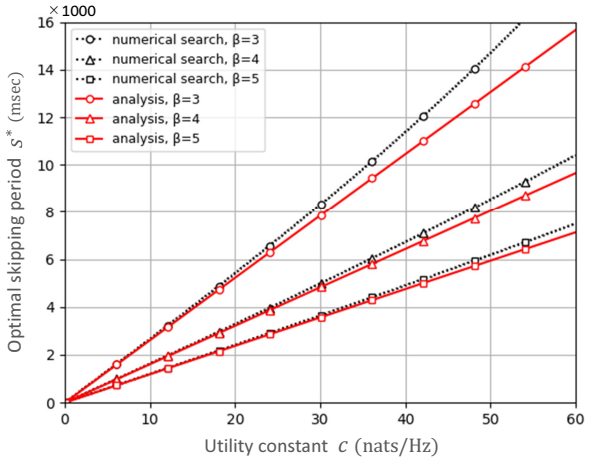

(b) s^* as a function of c.

Figure 3.2: The values of s^* in (3.16) with respect to the path-loss exponent β and the utility constant c in (3.15).

3.5 Comparison with other handover skipping schemes

We further investigate the optimal skipping period by conducting a comparison study with the two baseline schemes: the alternate HO skipping as the first baseline [9], and the topology-aware HO skipping[2] as the second

[2]We particularly choose the criteria for the topology-aware HO skipping as the chord length of a cell; HOs are not performed when the typical UE enters a cell whose chord length made by the UE's trajectory is less than the threshold $T > 0$.

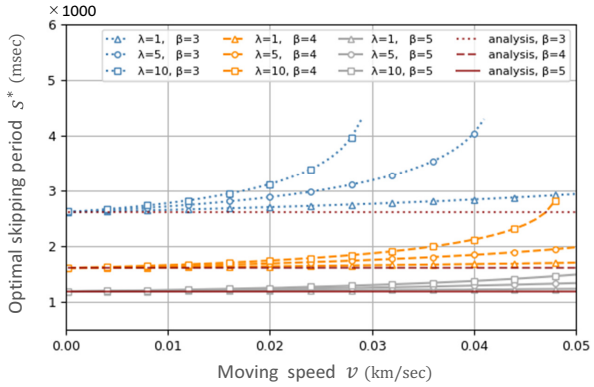

(a) s^* as a function of v with several patterns of λ and β, where $c = 10$ (nats /Hz) is fixed.

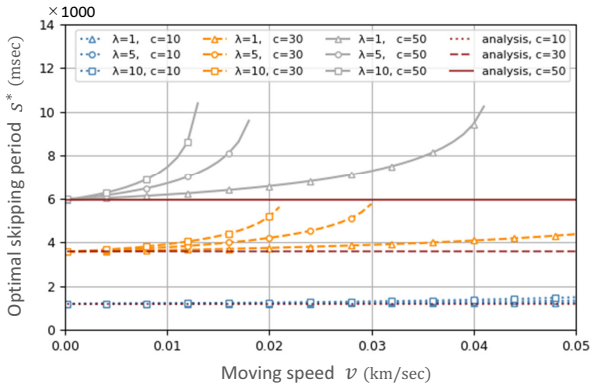

(b) s^* as a function of v with several patterns of λ and c, where $\beta = 5$ is fixed.

Figure 3.3: The values of s^* in (3.16) with respect to the moving speed v of the typical UE.

baseline [13]. We consider the utility metric defined in (3.2) for both the two baseline schemes and compare with the one of our proposed scheme, where the expected data rate and the HO rate in those baseline schemes are computed via simulations. As for the utility metric of our proposed scheme, we consider $\widetilde{\mathcal{U}}(s)$ given in (3.15) and regard s as the closest integer to s^* computed by the expression in (3.16), where the time unit is msec.

The result of the comparison is shown in Fig. 3.4. We see that our proposed scheme outperforms the alternate HO skipping scheme for exhibited values of λ and also outperforms the topology-aware HO skipping scheme particularly when λ is large. This is thought to be because our proposed scheme does not cause excessive degradation of the data rate for any λ, since the HO rate $1/s$ is at least ensured and the UE can refresh its connection every time

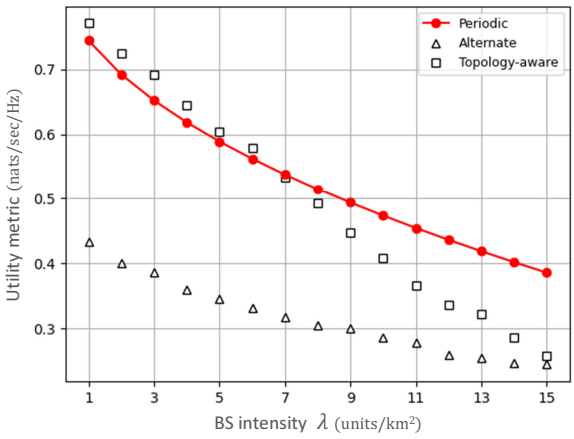

Figure 3.4: Comparison among the utility metrics of our proposed scheme (Periodic, in the graph legends) and the two baseline schemes (Alternate and Topology-aware, in the graph legends). Simulation results are exhibited discretely for the two baseline schemes, while numerical results are exhibited for the proposed scheme. The chord length threshold T in the topology-aware HO skipping scheme (the second baseline) is set as $T = 0.3$ (km). The other system parameters are fixed as $v = 0.01$ (km/sec), $c = 10$ (nats/Hz), and $\beta = 3$.

interval of s. That is, the HO rate could be managed for preventing the data rate degradation in our proposed scheme, which exhibits better performance results compared with those baseline HO skipping schemes depending on the value of λ.

3.6 Proof of Proposition 3.2

To obtain the first derivative of $\widetilde{\mathcal{U}}(\mathrm{s})$ in (3.15) with respect to s, we consider the Taylor expansion around $v = 0$, and ignore terms for which the order of v is greater than 2. Then, the first term of $\widetilde{\mathcal{U}}(s)$ yields

$$\begin{aligned}
&\frac{1}{v}\frac{\mathrm{d}}{\mathrm{d}s}\int_0^v \tau'(sw)\,\mathrm{d}w \\
&= \frac{\beta}{2v}\frac{\mathrm{d}}{\mathrm{d}s}\int_0^v\int_0^\infty \frac{1-\frac{2\pi\lambda z}{1+2z}s^2w^2}{\{1+(K_\beta z^{-1})^{\beta/2}\}(1+2z)} z^{-1}\mathrm{d}z\mathrm{d}w + o(v^2) \qquad as \quad v\to 0 \\
&\approx -\frac{2}{3}sv^2\pi\lambda\beta\int_0^\infty \frac{1}{1+(K_\beta z^{-1})^{\beta/2}}\cdot\frac{1}{(1+2z)^2}\mathrm{d}z. \qquad (3.17)
\end{aligned}$$

Regarding the second term of $\widetilde{\mathcal{U}}(s)$, we consider the asymptotical form of $\eta(sv)$ given in (3.12) under the condition that $v \approx 0$. Since $v \ll r$ yields $\sin^{-1}\left(\frac{sv\sin\theta}{w_{sv,r,\theta}}\right) \approx \sin^{-1}\left(\frac{sv\sin\theta}{r}\right)$, $\varrho(r,\theta|sv)$ in (3.13) is expressed as follows

$$\begin{aligned}
&\varrho(r,\theta|sv)\\
&\approx w_{sv,r,\theta}{}^2\left[\theta+\sin^{-1}\left(\frac{sv\sin\theta}{r}\right)\right]-r^2\theta+svr\sin\theta\\
&= w_{sv,r,\theta}{}^2\left[\theta+\frac{sv\sin\theta}{r}\right]-r^2\theta+svr\sin\theta+o(v^2)\\
&= -2svr(\theta\cos\theta-\sin\theta)+s^2v^2(\theta-\sin 2\theta)+o(v^2)\qquad as\quad v\to 0,
\end{aligned}$$

where the Maclaurin expansion of $\sin^{-1}\left(\frac{sv\sin\theta}{r}\right)$ is applied in the first equality, and (3.7) is used in the last equality. Substituting the above expression into (3.12) yields

$$\begin{aligned}
&\eta(sv)\\
&\approx 1-2\lambda\int_0^{\pi}\int_0^{\infty} r\mathrm{e}^{-\lambda\pi r^2}\\
&\quad\times \mathrm{e}^{2\lambda svr(\theta\cos\theta-\sin\theta)}\cdot \mathrm{e}^{-\lambda s^2v^2(\theta-\sin 2\theta)}\mathrm{d}r\mathrm{d}\theta+o(v^2)\\
&= -2\lambda\int_0^{\pi}\int_0^{\infty} r\mathrm{e}^{-\lambda\pi r^2}\Big[2\lambda svr(\theta\cos\theta-\sin\theta)\\
&\quad+\lambda s^2v^2\left\{2\lambda r^2(\theta\cos\theta-\sin\theta)^2-(\theta-\sin 2\theta)\right\}\Big]\mathrm{d}r\mathrm{d}\theta+o(v^2)\\
&= \frac{4\sqrt{\lambda}}{\pi}sv-\frac{15-\pi^2}{6\pi}\lambda s^2v^2+o(v^2)\qquad as\quad v\to 0,
\end{aligned}$$

where the Maclaurin expansion of the exponential form is applied in the first equality. Therefore, we have

$$\frac{\mathrm{d}}{\mathrm{d}s}\frac{c}{s}\eta(sv)\approx -\frac{15-\pi^2}{6\pi}c\lambda v^2. \tag{3.18}$$

From (3.17) and (3.18), we derive the asymptotical form of the first-order derivative of $\widetilde{\mathcal{U}}(\mathrm{s})$ as

$$\frac{\mathrm{d}}{\mathrm{d}s}\widetilde{\mathcal{U}}(s)\approx -\frac{2}{3}sv^2\pi\lambda\beta\int_0^{\infty}\frac{1}{1+(K_\beta z^{-1})^{\beta/2}}\cdot\frac{1}{(1+2z)^2}\mathrm{d}z+\frac{15-\pi^2}{6\pi}cv^2\lambda.$$

It follows from the expression above that the approximate form of the function $\widetilde{\mathcal{U}}(\mathrm{s})$ is concave and has only one peak because $\frac{\mathrm{d}}{\mathrm{d}s}\widetilde{\mathcal{U}}(\mathrm{s})$ is a linear function with respect to s, and $\frac{\mathrm{d}}{\mathrm{d}s}\widetilde{\mathcal{U}}(s)>0$ when s is sufficiently small and $\frac{\mathrm{d}}{\mathrm{d}s}\widetilde{\mathcal{U}}(s)<0$ when s is sufficiently large. Thus, the extreme point of $\widetilde{\mathcal{U}}(s)$ corresponds to the global maximum with respect to s.

Finally, solving $\frac{\mathrm{d}}{\mathrm{d}s}\widetilde{\mathcal{U}}(s)=0$ for s completes the proof.

3.7 Conclusion

We have discussed how to decide the length of the skipping period and have provided a simple computable expression of the skipping period which approximately gives a local maximum of the utility metric. Numerical comparison with other related HO skipping techniques have also shown that the proposed scheme is comparable to the others. Although we have considered here a simple mobility model on a homogeneous PPP network model, further development within more extended and generalized frameworks (e.g., HetNets with interference cancellation and/or the BS cooperation) would be expected for future work and one direction of the extensions is found in [18].

Chapter 4

An Extension to Heterogeneous Networks Using Poisson-Poisson Cluster Process

4.1 Introduction

Network densification is regarded as a promising approach to cope with the ever-growing traffic in the current fifth generation (5G) cellular networks [8]. In the densified cellular networks, miniaturized base stations (BSs), namely, small BSs (SBSs), play a key role in complementing the capacity for the traffic not sufficiently covered by macro BSs (MBSs) [45]. SBSs are often considered to be deployed as they form clusters for intensive improvement of the capacity around the hot spots and the dead zones [46, 47]. On the other hand, the network densification could cause frequent handovers (HOs), especially for mobile user equipments (UEs) passing through the area of the clustered SBSs.

During the process of an HO, a mobile UE exchanges signals with the serving BS and the target BS, which are connected via the core network. If the HOs are processed frequently, enormous signals could cause huge signaling overheads among those networks, which diminishes performance for the UE [11]. To mitigate those frequent HOs, HO skipping approaches have been proposed. HO skipping enables a UE to reduce the HO rate, whereas it may decrease the data rate because it demands the UE to maintain longer connection duration with a BS. Thus, the HO skipping presents a trade-off relation between the increased HO rate and the decreased data rate, and the

trade-off relation should be balanced to improve the performance for UEs.

Studies of performance analysis for user mobility in cellular networks have been extensively done in the literature. Among them, stochastic geometry-based approach have recently attracted researchers' interest [19,24,31]. While adopting cluster point processes for modeling the intensively deployed SBSs has gained much attention owing to the aforementioned background, the existing studies in this context are still few. In [48], they first analyzed the HO rate in a single-tier network where BSs are deployed according to a Poisson-Poisson cluster process (PPCP). Thereafter, they extend the result to a multi-tier heterogeneous network where either a Poisson point process (PPP) or a PPCP is adopted for the deployment in each tier, and considered the optimal tier selection for a moving UE by balancing the tradeoff between improving the data rate and reducing the HO rate. In [49], they proposed a modified random waypoint model based on the one proposed in [23]. Moreover, they considered a heterogeneous network that consist of three tiers, in one of which SBSs are deployed according to a PPCP, and derived the HO rate, the HO failure rate, and the ping-pong rate of a moving UE that follows the modified random waypoint model.

The technique of HO skipping has been investigated and analyzed by stochastic geometry approach, where the majority of the work consider to model the locations of BSs by a homogeneous PPP due to its simplicity and tractability [4]. Arshad et al. [9] proposed an HO skipping technique, in which a UE skips HOs under certain conditions. More precisely speaking, in their study, UE alternatively skips HOs along its moving trajectory. Moreover, the authors evaluated the performance via quantifying throughput of the UE in a PPP-based single-tier network. Thereafter, in [10], a velocity-aware HO skipping technique was analyzed in a PPP-based two-tier network. In [12,13], a topology-aware HO skipping technique was analyzed in a PPP-based single-tier network. In [50], a user-centric cooperative transmissions-based handover scheme, named the group-cell HO scheme, was proposed, and they developed a new framework of HO skippings based on their proposed group-cell HO scheme. In [16, 17], authors proposed a periodic HO skipping technique and evaluated it in a PPP-based single-tier network.

In our study, we consider a 2-tier heterogeneous cellular network, where macro and small BSs are respectively deployed by PPP and a PPCP. Real-world small BSs which tend to be deployed as clusters can be well represented by the PPCP. For modeling moving UEs, inspired by [16, 17], we employ a similar random walk-based model with a periodic HO skipping technique. Note that we introduce two distinct skipping period parameters unlike [16,17] since our network consists of two types of BSs. Based on this system model, we provide two analytical results in Section 4.3: *the exact expression of the*

HO rate and *the approximated expression of the expected data rate*. To the best of our knowledge, no HO skipping technique has yet been analyzed based on our network. Thus, these two analytical results are our main contributions. Moreover, based on the two analytical results, the efficiency of the HO skipping technique in our network is evaluated by comparing it with non-HO skipping counterpart in numerical experiments.

4.2 System model

4.2.1 Network model

As mentioned at the end of Section 4.1, our network consists of a macro BS tier and a small BS tier. Macro BSs (resp. Small BSs) are referred to as 1st (resp. 2nd) tier. Macro BSs are assumed to be deployed on $\mathbb{R}^2$ as a homogeneous PPP Φ_1 with intensity λ_1. All the macro BSs transmit signal power with the same level adopting a common spectrum bandwidth, and the power level is denoted by P_1. Small BSs are deployed as a PPCP Φ_2 by transmitting the same power level P_2, where we assume that Φ_2 has the isotropy. The isotropic PPCP $\Phi_2 = \Phi(\lambda_p, g, \bar{m})$ is defined as in Definition 1.4 of Chapter 1. As described in (1.1), Φ_2 consists of the offspring process C^z shifted by z for each $z \in \Psi_p$, and $\boldsymbol{x}_i \in z + C^z$, $i = 1, \cdots, M$, are conditionally i.i.d. with the probability density function (PDF) $g(\boldsymbol{x}_i - z)$.

Let $\boldsymbol{x}_k \in \mathbb{R}^2$ $(k \in \mathbb{N})$ denote an element of Φ_i $(i = 1, 2)$, expressing the position of either a macro or a small BS. Here, k is an index of the BS. We assume Rayleigh Fading and general power-law path-loss on downlinks while ignoring shadowing effects. Thus, the UE at $\boldsymbol{u} \in \mathbb{R}^2$ receives the following signal power at discrete time $t \in \mathbb{N}_0$ from a BS at $\boldsymbol{x} \in \mathbb{R}^2$: $P_{(\boldsymbol{x})} H_{\boldsymbol{x},t} \|\boldsymbol{x} - \boldsymbol{u}\|^{-\beta}$, where $H_{\boldsymbol{x},t}$ are i.i.d. random variables such that $H_{\boldsymbol{x},t} \sim \exp(1)$, representing the fading effect from the location $\boldsymbol{x}$. As for $P_{(\boldsymbol{x})}$, $P_{(\boldsymbol{x})} = P_1$ if $\boldsymbol{x} \in \Phi_1$, otherwise $P_{(\boldsymbol{x})} = P_2$. The symbol β (> 2) denotes the general path-loss exponent for both tiers. We then define the downlink Signal-to-Interference-plus-Noise Ratio (SINR) for UE at $\boldsymbol{u}$ when it receives signal power at the time t from BS at $\boldsymbol{x} \in \Phi_1 \cup \Phi_2$ as follows:

$$\mathsf{SINR}_{\boldsymbol{x},\boldsymbol{u}}(t) = \frac{P_{(\boldsymbol{x})} H_{\boldsymbol{x},t} \|\boldsymbol{x} - \boldsymbol{u}\|^{-\beta}}{I_{(\Phi_1 \cup \Phi_2) \setminus \boldsymbol{x},\boldsymbol{u}}(t) + \sigma^2}, \tag{4.1}$$

where $I_{(\Phi_1 \cup \Phi_2) \setminus \boldsymbol{x},\boldsymbol{u}}(t)$ denotes the interference power at time $t \in \mathbb{N}_0$ from all the BSs except the one at $\boldsymbol{x}$ when UE is at $\boldsymbol{u}$, and $\sigma^2 > 0$ denotes the noise

power. The interference power is given by

$$I_{(\Phi_1\cup\Phi_2)\setminus\boldsymbol{x},\boldsymbol{u}}(t) = \sum_{\boldsymbol{x}'\in(\Phi_1\cup\Phi_2)\setminus\boldsymbol{x}} P_{(\boldsymbol{x}')} H_{\boldsymbol{x}',t} \left\|\boldsymbol{x}'-\boldsymbol{u}\right\|^{-\beta}. \tag{4.2}$$

Eventually, $\log\left(1+\mathsf{SINR}_{\boldsymbol{x},\boldsymbol{u}}(t)\right)$ defines the instantaneous downlink data rate.

4.2.2 Mobility model for a moving user equipment

As for the network described in Section 4.2.1, a moving UE is modeled by a random walk with a periodic HO skipping technique explained as follows. Initially, the UE is at $S(0) \in \mathbb{R}^2$. For any $j \in \mathbb{N}$, at the beginning of the j-th movement, the UE is at $S(j-1) \in \mathbb{R}^2$. At the end of the movement, UE is at $S(j) \in \mathbb{R}^2$. During the j-th movement, the UE moves on straightly with constant velocity $V_j \in \mathbb{R}^2$, while it is always associated with the only one same BS. The velocities V_j, $j \in \mathbb{N}$ are assumed to be i.i.d. random vectors. In addition, such associated BS in the movement is decided by the following criterion: if a BS at $\boldsymbol{x}_{k_1^*}$ provides higher power to the UE at $S(j-1)$ than a BS at $\boldsymbol{x}_{k_2^*}$, UE will be associated with the BS at $\boldsymbol{x}_{k_1^*}$. Otherwise the BS at $\boldsymbol{x}_{k_2^*}$. Here, k_i^* $(i=1,2)$ denotes the index of BS which is the closest (with Euclidean metric) to the UE among i-th tier BSs. Moreover, if an i-th tier BS provides higher signal power to the UE at $S(j-1)$, UE is supposed to spend a constant $s_i \in \mathbb{N}$ units of time from $S(j-1)$ to $S(j)$, and then $S(j) = S(j-1) + s_i V_j$. Here, the periods of the time s_1 and s_2 are respectively called the *macro skipping period* and the *small skipping period*.

4.2.3 Performance metrics

We furthermore define the HO rate $\mathcal{H}(s_1,s_2,v)$ and the expected data rate $\mathcal{T}(s_1,s_2,v)$ for the UE attempting the periodic HO skipping scheme in our 2-tier network model. Following the previous chapters, $\mathcal{H}(s_1,s_2,v)$ and $\mathcal{T}(s_1,s_2,v)$ are defined as follows

$$\begin{aligned}
\mathcal{H}(s_1,s_2,v) &= \lim_{m\to\infty} \frac{\mathsf{E}[\zeta(0,m)]}{m},\\
\mathcal{T}(s_1,s_2,v) &= \lim_{m\to\infty} \frac{1}{m}\sum_{t=0}^{m-1} \mathsf{E}[\log(1+\mathsf{SINR}_{\boldsymbol{x},\boldsymbol{u}}(t))],
\end{aligned}$$

where $\zeta(0,m)$ denotes the number of HOs executed by the typical UE up to the time $m \in \mathbb{N}$, and $\mathsf{SINR}_{\boldsymbol{x},\boldsymbol{u}}(t)$ is given in (4.1).

4.3 Analyses

We aim to analyze expectations of the HO rate and the expected data rate defined in the preceding section. To do so, it suffices to analyze the two expectations in the 1st movement with $S(0) = \boldsymbol{o}$ and $V_1 = (v, 0)^\top$, where we assume $v \geq 0$ is fixed. The reason is due to the stationatiry of Φ_1, Ψ_p and the isotropy of Φ_1, Ψ_p, g; see the proof of Theorem 1 in [17]. For these analyses, we use $\mathsf{SINR}_{\boldsymbol{x},u}(t)$ instead of $\mathsf{SINR}_{\boldsymbol{x},\boldsymbol{u}}(t)$ in (4.1), where $\boldsymbol{u} = (u, 0)^\top$ and $u \geq 0$. In addition, $I_{\cdot,u}(t)$ is used instead of the left term in (4.2). Moreover, while we employ a polar coordinate system, a position $\boldsymbol{x} \in \mathbb{R}^2$ is expressed by (x, θ) where $x = \|\boldsymbol{x}\|$ and $\theta \in [0, 2\pi)$.

4.3.1 Handover rate analysis

Proposition 4.1. *The HO rate $\mathcal{H}(s_1, s_2, v)$ is given by* (4.3)*,*

$$\mathcal{H}(s_1, s_2, v_j) = \frac{2\pi\lambda_1}{\kappa(s_1, s_2)} \int_0^\infty r \mathrm{e}^{-\lambda_1 \pi r^2} A_1(r) \left[1 - \frac{1}{\pi} \int_0^\pi D_1(r, s_1 v_j, \theta) \mathrm{d}\theta \right] \mathrm{d}r$$
$$+ \frac{\bar{m}}{\kappa(s_1, s_2)} \int_0^\infty \mathrm{e}^{-\lambda_1 \pi \hat{P}_{2,1}^2 r^2} A_2(r) \left[B(r) - \frac{1}{\pi} \int_0^\pi C(r, s_2 v_j, \theta) D_2(r, s_2 v_j, \theta) \mathrm{d}\theta \right] \mathrm{d}r, \quad (4.3)$$

where

$$A_i(r) = \exp\left(-2\pi\lambda_p \int_0^\infty z \left\{ 1 - \mathrm{e}^{-\bar{m} F_d(\hat{P}_{i,2} r | z)} \right\} \mathrm{d}z \right), \quad (4.4)$$

$$B(r) = 2\pi\lambda_p \int_0^\infty z \, f_d(r \,|\, z) \, \mathrm{e}^{-\bar{m} F_d(r|z)} \mathrm{d}z, \quad (4.5)$$

$$C(r, \ell, \theta) = 2\lambda_p \int_0^\infty z \, f_d(r \,|\, z) \, \mathrm{e}^{-\bar{m} F_d(r|z)}$$
$$\times \int_0^\pi \exp\left(-\bar{m} \int_{\mathcal{D}_{2,2}(r,\ell,\theta)} g(\boldsymbol{x} - \boldsymbol{z}) \mathrm{d}\boldsymbol{x} \right) \mathrm{d}\theta \mathrm{d}z, \quad (4.6)$$

$$D_i(r, \ell, \theta) = \exp\left(-\lambda_1 \,|\, \mathcal{D}_{i,1}(r, \ell, \theta) \,| - 2\lambda_p \int_0^\infty z \, \mathrm{e}^{-\bar{m} F_d(\hat{P}_{i,2} r | z)} \right.$$
$$\left. \times \int_0^\pi \left\{ 1 - \exp\left(-\bar{m} \int_{\mathcal{D}_{i,2}(r,\ell,\theta)} g(\boldsymbol{x} - \boldsymbol{z}) \mathrm{d}\boldsymbol{x} \right) \right\} \mathrm{d}\theta \mathrm{d}z \right), \quad (4.7)$$

and $\mathcal{D}_{i,j}(r, \ell, \theta)$, $i, j = 1, 2$, is a two dimensional region defined by

$$\mathcal{D}_{i,j}(r, \ell, \theta) = b\left((\ell, 0), \hat{P}_{i,j} \omega_{r,\ell,\theta} \right) \cap b(\boldsymbol{o}, \hat{P}_{i,j} r)^c, \quad (4.8)$$

with $\hat{P}_{i,j} = (P_j/P_i)^{1/\beta}$ *and* $\omega_{r,u,\theta} = \sqrt{r^2+u^2-2ru\cos\theta}$. *Moreover,* $\kappa(s_1, s_2)$ *denotes the expected length of a skipping period, which is given by*

$$\kappa(s_1, s_2) = s_1(1 - \mathsf{P}(\mathcal{S}_2)) + s_2\mathsf{P}(\mathcal{S}_2), \tag{4.9}$$

with

$$\mathsf{P}(\mathcal{S}_2) = 2\pi\bar{m}\lambda_p \int_0^\infty \mathrm{e}^{-\pi\lambda_1\hat{P}_{2,1}^2 r^2} \int_0^\infty f_d(r\,|\,z) \exp\Big(-\bar{m}F_d(r\,|\,z)\Big) z\mathrm{d}z \\ \times \exp\left(-2\pi\lambda_p \int_0^\infty \Big(1 - \exp\Big(-\bar{m}F_d(r\,|\,z)\Big)\Big) z\mathrm{d}z\right)\mathrm{d}r.$$

Remark 4.1. *We recall that* $f_d(r \mid \boldsymbol{z})$ *and* $F_d(r \mid \boldsymbol{z})$ *in the above expressions respectively denote the conditional PDF of the distance* $r = \|\boldsymbol{x}\|$ *of an offspring point* $\boldsymbol{x} \in \Phi(\lambda_p, g, \bar{m})$ *from the origin given its cluster center at* $\boldsymbol{z} \in \Psi_p$, *and its CDF. Their specific expressions when the PPCP* Φ_2 *is specified as Thomas Cluster Process (TCP) or Mattern Cluster Process (MCP) are provided in [7].*

Proof. For $i = 1, 2$, let $\mathcal{S}_i$ and H_i^c respectively denote the events that the UE is associated with the i-th tier in the 1st movement, and that an HO does not occur at the end of the movement. Then, we have

$$\mathcal{H}(s_1, s_2, v) = \frac{\mathsf{E}[N(s_1, s_2, v)]}{\kappa(s_1, s_2)}, \tag{4.10}$$

where $N(s_1, s_2, v)$ denotes the number of HOs that occur in a certain skipping period, and $\kappa(s_1, s_2)$ is given in (4.9). Here, $\mathsf{E}[N(s_1, s_2, v)]$ is given by

$$\mathsf{E}[N(s_1, s_2, v)] = \sum_{i=1}^{2} \big(1 - \mathsf{P}(H_i^c\,|\,\mathcal{S}_i)\big)\mathsf{P}(\mathcal{S}_i). \tag{4.11}$$

Let $r = \|\boldsymbol{x}_{k_i^*}\|$ denote the magnitude of the UE's associated BS in the event $\mathcal{S}_i$. Conditioned on the parent PP Ψ_p, the PDF of r is obtained from Lemma 4 of [7], that is

$$f_c(r\,|\,\mathcal{S}_i, \Psi_p) = \frac{\Lambda(i)}{\mathsf{P}(S_i\,|\,\Psi_p)} \mathrm{e}^{-\lambda_1\pi\hat{P}_{i,1}^2 r^2} \prod_{z\in\Psi_p} \mathrm{e}^{-\bar{m}F_d(\hat{P}_{i,2}r|z)}$$

where $\big(\Lambda(1),\, \Lambda(2)\big) = \big(2\pi\lambda_1 r,\, \bar{m}\sum_{z\in\Psi_p} f_d(r\,|\,z)\big)$, and

$$\mathsf{P}(S_i\,|\,\Psi_p) = \int_0^\infty \Lambda(i)\, \mathrm{e}^{-\lambda_1\pi\hat{P}_{i,1}^2 r^2} \prod_{z\in\Psi_p} \mathrm{e}^{-\bar{m}F_d(\hat{P}_{i,2}r|z)}\mathrm{d}r. \tag{4.12}$$

Therefore, we have

$$\begin{aligned}
&\mathsf{P}(\mathcal{S}_i)\mathsf{P}(H_i^c \,|\, \mathcal{S}_i) = \mathsf{E}[\mathsf{P}(\mathcal{S}_i \,|\, \Psi_p)\mathsf{P}(H_i^c \,|\, \mathcal{S}_i, \Psi_p)] \\
&= \frac{1}{2\pi}\int_0^{2\pi}\int_0^{\infty} \mathrm{e}^{-\lambda_1 \pi \hat{P}_{i,1}^2 r^2} \\
&\quad \times \mathsf{E}\left[\Lambda(i)\prod_{z\in\Psi_p} \mathrm{e}^{-\bar{m}F_d(\hat{P}_{i,2}r|z)}\mathsf{P}(H_i^c \,|\, r, \theta, \mathcal{S}_i, \Psi_p)\right]\mathrm{d}r\mathrm{d}\theta. \qquad (4.13)
\end{aligned}$$

We next let $H_{i,j}^c$, $i, j = 1, 2$, denote the event that there is no need to perform HOs from the i-th tier to the j-th tier at the end of the movement. Note that under the condition of $\mathcal{S}_i$ and $\boldsymbol{x}_{k_i^*} = (r, \theta)$, the event $H_{i,j}^c$ occurs if and only if there are no BSs of the j-th tier offering stronger signal power for the UE at the position $(s_i v, 0)$ than the BS at the polar coordinate (r, θ). Also note that any BSs of the j-th tier could not be allocated inside the circle region $b(\boldsymbol{o}, \hat{P}_{i,j} r)$ under the condition of $\mathcal{S}_i$ and $\boldsymbol{x}_{k_i^*} = (r, \theta)$. Since Φ_1 and Φ_2 conditioned on Ψ_p are respectively PPPs with the intensities λ_1 and $\bar{m}\sum_{z\in\Psi_p} f(\boldsymbol{x} \mid \boldsymbol{z})$ (see Proposition 1.1), $\mathsf{P}(H_i^c \mid r, \theta, \mathcal{S}_i, \Psi_p) = \prod_{k=1,2}\mathsf{P}(H_{i,k}^c \mid r, \theta, \mathcal{S}_i, \Psi_p)$ is given as follows

$$\begin{aligned}
&\mathsf{P}(H_i^c \,|\, r, \theta, \mathcal{S}_i, \Psi_p) \\
&= \mathrm{e}^{-\lambda_1 |\mathcal{D}_{i,1}(r, s_i v, \theta)|} \prod_{z\in\Psi_p} \exp\left(-\bar{m}\int_{\mathcal{D}_{i,2}(r, s_i v, \theta)} f(\boldsymbol{x} \,|\, \boldsymbol{z})\mathrm{d}\boldsymbol{x}\right), \qquad (4.14)
\end{aligned}$$

where $\mathcal{D}_{i,j}(r, s_i v, \theta)$ is in (4.8) and the norm $|\cdot|$ denotes the area of a region. Substituting (4.11), (4.12), (4.13), and (4.14) into (4.10), and applying the probability generating functional (PGFL) and the sum-product functional (SPFL) (see Lemma 5 and 6 of [7]) to the parent PPP Ψ_p, we obtain (4.3). The rest part marely consists of algebraic manipulations, so it is omitted. □

4.3.2 Data rate analysis

Proposition 4.2. *The expected data rate $\mathcal{T}(s_1, s_2, v)$ is approximately given by*

$$\begin{aligned}\mathcal{T}(s_1,s_2,v) = \frac{2\lambda_1}{\kappa(s_1,s_2)} \sum_{t=0}^{s_1-1} \int_0^\infty r\, \mathrm{e}^{-\lambda_1 \pi r^2 - \frac{w_{r,tv,\theta}\, y}{P_1}\sigma^2} A_1(r) \\ \times \int_0^\pi \int_0^\infty \frac{\mathcal{J}_1(y,\theta,r,tv)\mathcal{K}_1(y,\theta,r,tv)}{1+y} \mathrm{d}y\mathrm{d}\theta\mathrm{d}r \\ + \frac{\bar{m}}{\kappa(s_1,s_2)} \sum_{t=0}^{s_2-1} \int_0^\infty \mathrm{e}^{-\lambda_1 \pi \hat{P}_{2,1}^2 r^2 - \frac{w_{r,tv,\theta}\, y}{P_2}\sigma^2} A_2(r) B(r) \\ \times \frac{1}{\pi} \int_0^\pi \int_0^\infty \frac{\mathcal{J}_2(y,\theta,r,tv)\mathcal{K}_2(y,\theta,r,tv)}{1+y} \mathrm{d}y\mathrm{d}\theta\mathrm{d}r, \end{aligned} \tag{4.15}$$

where $A_i(r)$ and $B(r)$ are respectively given in (4.4) *and* (4.5)*, and*

$$\begin{aligned}\mathcal{J}_i(y,\theta,r,u) = \exp\Bigg(-2\lambda_1 \Bigg\{ K_\beta \hat{P}_{i,1}^2 w_{r,u,\theta}^2\, y^{\frac{2}{\beta}} \\ - \int_0^{\hat{P}_{i,1} r + u} \widetilde{R}(x, \hat{P}_{i,1} r, u) \left[1 + \frac{1}{y}\left(\frac{x}{\hat{P}_{i,1} w_{r,u,\theta}}\right)^\beta\right]^{-1} x\mathrm{d}x \Bigg\}\Bigg), \\ \mathcal{K}_i(y,\theta,r,u) \approx \exp\Bigg(-2\pi\lambda_p \int_0^\infty z \Bigg\{ 1 - \exp\Bigg(-\bar{m} \int_0^\infty f_d(x \mid z) \\ \times \left[1 + \frac{1}{y}\left(\frac{x}{\hat{P}_{i,2} w_{r,u,\theta}}\right)^\beta\right]^{-1} \mathrm{d}x\Bigg)\Bigg\} \mathrm{d}z\Bigg),\end{aligned}$$

with

$$K_\beta = \frac{\pi^2}{\beta} \csc\frac{2\pi}{\beta}, \quad \widetilde{R}(x,h,u) = \begin{cases} \pi, & (u=0) \\ \cos^{-1}\left(-1 \vee \frac{x^2 - h^2 + u^2}{2xu} \wedge 1\right), & (u>0) \end{cases} \tag{4.16}$$

Proof. Similar to the proof of Proposition 4.1, we have

$$\mathcal{T}(s_1,s_2,v) = \frac{\mathsf{E}[T(s_1,s_2,v)]}{\kappa(s_1,s_2)}, \tag{4.17}$$

where $T(s_1, s_2, v)$ denotes the amount of received data in a certain period,

and $\kappa(s_1, s_2)$ is given in (4.9). Here, $\mathsf{E}[T(s_1, s_2, v)]$ is given by

$$\begin{aligned}
&\mathsf{E}[T(s_1, s_2, v)] \\
&= \sum_{i=1}^{2} \mathsf{P}(\mathcal{S}_i)\mathsf{E}[T(s_1, s_2, v) \,|\, \mathcal{S}_i] \\
&= \frac{1}{2\pi}\sum_{i=1}^{2}\int_0^{2\pi}\int_0^{\infty} \mathrm{e}^{-\lambda_1 \pi \bar{P}_{1,i}^2 r^2} \sum_{t=0}^{s_i-1} \mathsf{E}\Bigg[\Lambda(i)\prod_{z\in\Psi_p} \mathcal{I}_{2,i}(r \,|\, z) \\
&\qquad\qquad \times \mathsf{E}[\log(1+\mathsf{SINR}_{\boldsymbol{x}_{k_i^*},tv}(t)) \,|\, r, \theta, \mathcal{S}_i, \Psi_p]\Bigg] \mathrm{d}r\mathrm{d}\theta. \qquad (4.18)
\end{aligned}$$

We consider to analyze $\mathsf{E}[\ln\left(1+\mathsf{SINR}_{\boldsymbol{x}_{k_i^*},u}(t)\right) \mid r, \theta, \mathcal{S}_i, \Psi_p]$ for $u \geq 0$, $t \in \mathbb{N}$, $i = 1, 2$. Recall that $\boldsymbol{x}_{k_i^*} = (r, \theta)$ denotes the nearest point of $\boldsymbol{\Phi}_i$ from the origin, and let $\mathcal{L}_{\cdot,u}$ denote the Laplace transform of the interference $I_{\cdot,u}$ conditioned on Ψ_p. Using (7) in [4], the expected data rate is expressed by the Laplace transform, that is,

$$\begin{aligned}
&\mathsf{E}\left[\ln\left(1+\mathsf{SINR}_{\boldsymbol{x}_{k_i^*},u}(t)\right) \,|\, r, \theta, \mathcal{S}_i, \Psi_p\right] \\
&= \int_0^{\infty} \mathrm{e}^{-c_i(y)\sigma^2} \mathcal{L}_{\Phi_1\cup\Phi_2\setminus\boldsymbol{x}_{k_i^*},u}\big(c_i(y)\big)\mathrm{d}y \\
&= \int_0^{\infty} \mathrm{e}^{-c_i(y)\sigma^2} \mathcal{L}_{\Phi_1\cap b(0,\bar{P}_{1,i}r)^c,u}\big(c_i(y)\big)\mathcal{L}_{\Phi_2\cap b(0,\bar{P}_{2,i}r)^c,u}\big(c_i(y)\big)\mathrm{d}y, \qquad (4.19)
\end{aligned}$$

where $c_i(y) = \omega_{r,u,\theta}(\mathrm{e}^y - 1)/P_i$, and the last equality follows from the mutual independence between $\boldsymbol{\Phi}_1$ and $\boldsymbol{\Phi}_2$.

Regarding $\mathcal{L}_{\Phi_1\cap b(0,v)^c,u}\big(c_i(y)\big)$, $v \geq 0$, since $\boldsymbol{\Phi}_1$ is a homogeneous PPP with the intensity λ_1, the analysis result is obtained in the proof of Lemma 1 in [17], which is

$$\begin{aligned}
&\mathcal{L}_{\Phi_1\cap b(0,v)^c,u}(c_i(y)) \\
&= \mathrm{e}^{-2\lambda_1\left(K_\beta P_1^{2/\beta} c_i(y)^{2/\beta} - \int_0^{u+v} \widetilde{R}(x,v,u)\frac{x}{1+P_1^{-1}c_i(y)^{-1}x^\beta}\mathrm{d}x\right)}, \qquad (4.20)
\end{aligned}$$

where K_β and $\widetilde{R}(x, v, u)$ are given in (4.16). As for $\mathcal{L}_{\Phi_2\cap b(0,v)^c,u}\big(c_i(y)\big)$, $v \geq 0$, since its analysis induces much complexity, we introduce an approximation similar to Proposition 4.1: we regard interfering BSs as assigned over entire $\mathbb{R}^2$ by another independent PPCP $\boldsymbol{\Phi}_2'$ whose parent process Ψ_p' and the offspring process are identical to ones of $\boldsymbol{\Phi}_2$. By this approximation, since $\boldsymbol{\Phi}_2'$ conditioned on Ψ_p' follows an inhomogeneous PPP with the intensity

$\bar{m}\sum_{z\in\Psi'_p} f(\boldsymbol{x}\,|\,\boldsymbol{z})$ (see Proposition 1.1), $\mathcal{L}_{\Phi_2\cap b(0,v)^c,u}\big(c_i(y)\big) \approx \mathcal{L}_{\Phi'_2,u}\big(c_i(y)\big)$ is given as follows

$$\begin{aligned}
&\mathcal{L}_{\Phi_2\cap b(0,v)^c,u}\big(c_i(y)\big)\\
&\approx \mathsf{E}\Bigg[\exp\Big(-c_i(y)\sum_{\boldsymbol{x}\in\Phi'_2} P_2\, H_{\boldsymbol{x},t}\|\boldsymbol{x}-\boldsymbol{u}\|^{-\beta}\Big)\,\Big|\, r,\theta,\mathcal{S}_i,\Psi_p\Bigg]\\
&= \mathsf{E}\Bigg[\prod_{\boldsymbol{x}\in\Phi'_2}\frac{1}{1+c_i(y)P_2\|\boldsymbol{x}\|^{-\beta}}\,\Big|\, r,\theta,\mathcal{S}_i,\Psi_p\Bigg]\\
&= \prod_{z\in\Psi'_p}\exp\Bigg(-\bar{m}\int_0^\infty \frac{f_d(x\,|\,z)}{1+c_i(y)^{-1}P_2^{-1}x^\beta}\mathrm{d}x\Bigg), \qquad (4.21)
\end{aligned}$$

where the shift-invariance of the parent PP Ψ'_p and the Laplace transform of $H_{\boldsymbol{x},t}\sim\exp(1)$ are applied in the first equality, and the PGFL of an inhomogeneous PPP and Lemma 1 of [7] are applied in the last equality. By substituting (4.18), (4.19), (4.20), and (4.21) into (4.17), applying the PGFL and the SPFL to the mutually independent PPs Ψ_p and Ψ'_p, and doing some algebraic manipulations like the preceding proposition, we obtain (4.15). □

4.4 Evaluation of transmission performance

We conduct two numerical experiments referred to as Expt1 and Expt2. See results of Expt1 in (a) and (b) of Fig.4.1, and results of Expt2 in (c) of Fig.4.2. The purpose of Expt1 is to evaluate the exact result of $\mathcal{H}(s_1,s_2,v)$ in (4.3) and the approximated result of $\mathcal{T}(s_1,s_2,v)$ in (4.15) by comparing with simulation. The purpose of Expt2 is to compare the two following scenarios. In Scenario 0, we employ a random walk-based UE with non-HO skipping in our network model: see Section 4.2.1. We note that the UE is, via performing HOs, always associated with a BS that provides the highest signal power. In Scenario 1, a UE model described in Section 4.2.2 is employed in the same network as Scenario 1. For both Expt1 and Expt2, PPCP Φ_2 is defined via Matern cluster process (MCP) having the cluster radius r_d; see Definition 4 of [7], and we respectively set 1.0 (units/km^2), 5, 0.1 (km), 1000 and 4 as λ_1, $\bar{m}$, r_d, P_1/P_2 and β.

Additionally for Expt1, we respectively fix s_1 and v to 20 (sec) and 0.02 (km/sec), while regarding s_2 and λ_p as variables. As we can see in (a) and (b) of Fig.4.1, the horizontal axes represent values of s_2 (sec). The vertical axes in (a) and (b) respectively express $\mathcal{H}(s_1,s_2,v)$ (/sec) and $\mathcal{T}(s_1,s_2,v)$ (nats/sec/Hz). All the twelve curves are functions of s_2 and λ_p, where λ_p is fixed to 5, 10, or 15. In (a) (resp. (b)), the red curves represent the

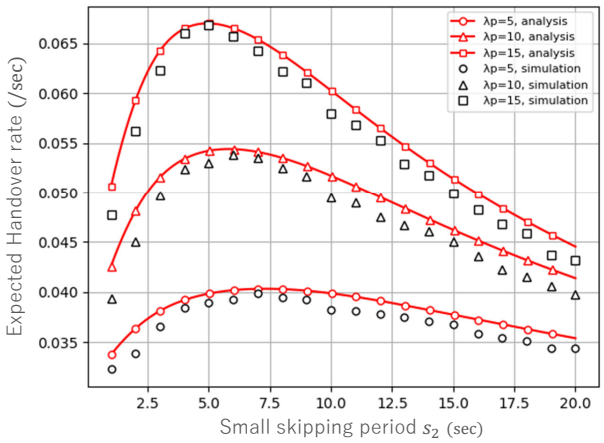

(a) $\mathcal{H}(s_1, s_2, v)$ as a function of s_2.

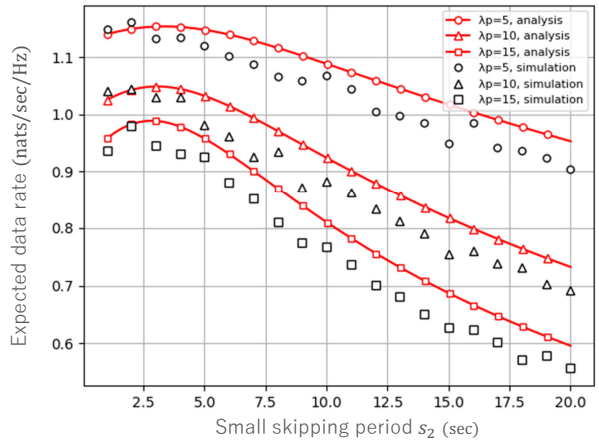

(b) $\mathcal{T}(s_1, s_2, v)$ as a function of s_2.

Figure 4.1: (a) and (b) correspond to results of Expt1. In (a) (resp. (b)), we compare the analysis results of the HO rate (resp. the expected data rate) with the simulation results. The analysis results are expressed by red curves in (a) and (b). We here fix s_1 to 20.

analytical results of $\mathcal{H}(s_1, s_2, v)$ (resp. $\mathcal{T}(s_1, s_2, v)$) defined via (4.3) (resp. (4.15)), which are computed via the traditional trapezoidal integral method. The black curves in (a) (resp. (b)) represent the values of $\mathcal{H}(s_1, s_2, v)$ (resp. $\mathcal{T}(s_1, s_2, v)$), which are obtained via Monte Carlo simulation with the average of 10000 independent samples.

On the other hand, as for Expt2, we respectively fix s_1 and s_2 to 20 (sec) and 10 (sec), while regarding v (km/sec) and λ_p as variables. To evaluate the efficiency of Scenario $j \in \{0, 1\}$, following [17], we introduce the following *utility metric*: $\mathcal{U}_j(s_1, s_2, v) = \mathcal{T}_j(s_1, s_2, v) - c\mathcal{H}_j(s_1, s_2, v)$. Here for $j = 1$,

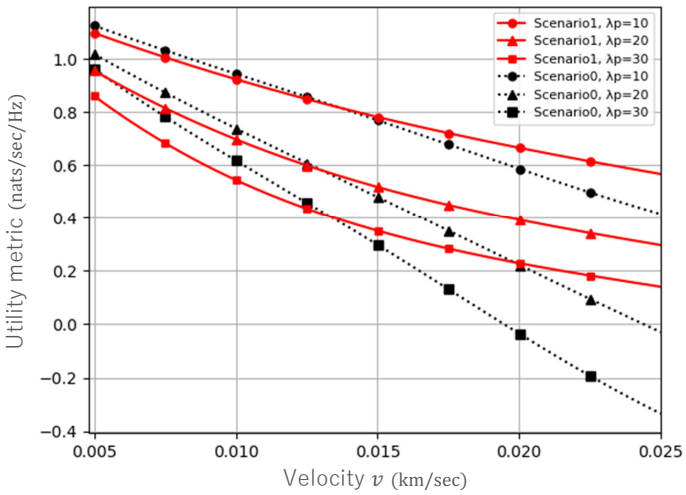

Figure 4.2: The result of Expt2. Based on the utility metric, we compare Scenario 0 (non HO skipping) with Scenario 1 (periodic HO skipping). The black and red curves respectively represent $\mathcal{U}_0(s_1, s_2, v)$ and $\mathcal{U}_1(s_1, s_2, v)$. We also respectively set 20 and 10 as skipping periods s_1 and s_2 in Scenario 2.

$\mathcal{T}_j(s_1, s_2, v)$ (nats/sec/Hz) and $\mathcal{H}_j(s_1, s_2, v)$ (/sec) are respectively defined by (4.15) and (4.3). For $j = 0$, $\mathcal{T}_j(s_1, s_2, v)$ (resp. $\mathcal{H}_j(s_1, s_2, v)$) is the expectation of total downlink data rate (resp. the expectation of the number of HOs) per second under Scenario 0. The symbol c (nats/Hz) denotes the cost of HO and is fixed to 5. In Fig.4.2, the horizontal axis represents the value of v. All the six curves are functions of v and λ_p, where λ_p is fixed to either 10, 20, or 30. The black curves represent the function $\mathcal{U}_0(s_1, s_2, v)$, whose values are obtained via the simulation. The red curves express the function $\mathcal{U}_1(s_1, s_2, v)$.

In (a) of Fig.4.1, we see that the analytical results of $\mathcal{H}(s_1, s_2, v)$ well correspond to the simulation results only with some small gaps. The reason of the gaps mainly come from the instability of the trapezoidal integral method we applied in the computation. Moreover, we see that $\mathcal{H}(s_1, s_2, v)$ is increasing in s_2 when s_2 is small. This is because $\mathsf{E}[N(s_1, s_2, v)]$, the numerator in (4.10), increases in s_2, whereas the effect of the increase of $\kappa(s_1, s_2)$, the denominator in (4.10), is comparatively small particularly when s_1 is large (see (4.9)). On the other hand, $\mathcal{H}(s_1, s_2, v)$ is decreasing in s_2 when s_2 is large. This is because $\mathsf{E}[N(s_1, s_2, v)]$ converges to 1 as s_2 increases, and the effect of the increase becomes comparatively small. In (b) of Fig.4.1, we observe that our analytical results correspond with the simulation results although some gaps exist. The reason of the gaps mainly comes from the effect of the

approximation introduced in the analysis of $\mathcal{T}(s_1, s_2, v)$. Furthermore, similar to Fig.4.1(a), we see that $\mathcal{T}(s_1, s_2, v)$ is increasing in s_2 when s_2 is small, and is decreasing in s_2 when s_2 is large. The reason is similar to the one for $\mathcal{H}(s_1, s_2, v)$; that is, the effect of the increase of $\mathsf{E}[T(s_1, s_2, v)]$ in (4.17) is large compared to $\kappa(s_1, s_2)$ when s_2 is small, and the effect gradually becomes little.

As for Fig.4.2, we observe that the faster the velocity v becomes, the better the periodic HO skipping technique outperforms non-HO skipping counterpart. We furthermore would like to emphasize that there exists (v, λ_p) such that $\mathcal{U}_1(s_1, s_2, v) > 0$ and $\mathcal{U}_1(s_1, s_2, v) > \mathcal{U}_0(s_1, s_2, v)$. For examples, $(v, \lambda_p) = (0.015, 30)$ and $(0.020, 20)$. Therefore in some cases, in the PPCP-based network, our proposed HO skipping scheme outperforms the non-HO skipping scheme for UE.

Remark 4.2. *Currently in cellular networks, under a cloud radio access network umbrella, decoupling control plane and user plane is considered to reduce the HO rate and control burden* [51]. *In this architecture, UEs associated with a small BS tier can receive data packets from a nearby small BS while being controlled via a farther macro BS, which enables to mitigate handover delays for HOs among small BSs* [52]. *While the constant c is considered for the cost of all kinds of HOs in our model, to consider different costs for such HOs in a small BS tier should be expected, which is left for future work.*

4.5 Conclusion

In this study, we focus on a 2-tier heterogeneous cellular network. Here, the 1st tier BSs are deployed as a homogeneous PPP, while the 2nd tier BSs are deployed as a PPCP. In this network, we consider a random walk-based UE with periodic HO skipping technique. Then, we analyze the expected HO rate and data rate by introducing approximations. The analytical results are respectively shown in (4.3) and (4.15). As we can see in (a) and (b) of Fig.4.1, the two obtained results approximate the corresponding exact values well. Moreover, we evaluate the efficiency of the periodic HO skipping technique in the network by comparing it with the non-HO skipping counterpart. The efficiency is quantized by the utility function. From the comparison result shown in Fig.4.2, we can have a deeper insight under what conditions the periodic HO skipping scheme in the network outperforms the non-HO skipping scheme, and also vice versa.

Chapter 5

Conclusion

5.1 Summary

In this thesis, we have proposed yet another HO skipping scheme, periodic HO skipping and investigated the performance in the proposed periodic HO skipping scheme via stochastic geometric analysis.

The studies in Chapter 2 and 3 have been conducted under the model of single-tier downlink cellular networks where BSs are allocated according to homogeneous PPP. We derived theoretical expressions of the two metrics: the expected data rate and the HO rate for a moving UE that performs the periodic HO skipping. On the basis of these theoretical results, we have studied transmission performance of a moving UE using the two metrics, under the model of the periodic HO skipping. From our analysis, we have found that the transmission performance in the periodic HO skipping scenario can outperform the non-skipping scenario when the moving speed of a UE is sufficiently large. Moreover, we have found that there is a local maximum of the transmission performance with respect to the skipping period of a UE. We have also investigated to derive a theoretical expression of the skipping period that gives the maximum, and conducted the performance comparison among other sophisticated HO skipping techniques.

The study in Chapter 4 has been conducted under the model of a two-tier heterogeneous cellular network, where the macro BSs and the small BSs are assumed to be deployed as a homogeneous PPP and a PPCP, respectively. Based on this network, we consider a random walk-based UE with periodic HO skipping technique. Then, we separately analyze the expected HO rate and the expected data rate by introducing certain approximations. Moreover, we evaluate the efficiency of the periodic HO skipping scheme by comparing it with the scenario of non-HO skipping, and successfully verify the efficiency

of the periodic HO skipping scheme in the two-tier network model.

5.2 Directions of future works

The studies in Chapter 2 and 3 have various points that need extension. For example, we considered a deterministic length of the skipping period, which could be enhanced to the random skipping period. Although we focused on optimizing the performance of a single user, incorporating multiple users in this model is essential for capacity management and load balancing in cellular networks. Furthermore, in our experiment, we gave the utility constant $c > 0$ as a hyperparameter, while it could be estimated from the implementation of cellular networks since it represents the cost of an HO.

In Chapter 4, studies of the transmission performance for the UE we gave are very limited. Especially, the optimal skipping period is not studied. Evaluation of the optimal skipping period in 2-tier cellular networks is of primal interest. Besides, in the experiment of the performance comparison, we considered a common utility constant in all kinds of HOs occuring in the 2-tier network model. However, to consider distinct utility constants between intra-tier HOs and inter-tier HOs should be expected. Moreover, the costs of intra-tier HOs among MBSs and SBSs should also be different (see Remark 4.2). To introduce those different HO costs is expected for future work. On the other hand, the given analytical results of the performance metrics have complex forms, so that remedies for mitigating that complexity would be expected, through such as approximate analysis or heuristic analysis.

For further study, we could consider incorporating the current wireless technologies in 5G, such as the inter-cell interference coordination [53], into the periodic HO skipping scheme. Moreover, this HO skipping scheme might contribute to the HO management problem in the unmanned aerial vehicle-assisted cellular networks [54] and the beam management problem in the millimeter-wave cellular networks [55].

Bibliography

[1] F. Baccelli, B. Blaszczyszyn, and M. Karray, "Random measures, point processes, and stochastic geometry," https://hal.inria.fr/hal-02460214, 2020.

[2] S. N. Chiu, D. Stoyan, W. S. Kendall, and J. Mecke, *Stochastic Geometry and its Applications*, 3rd ed., Wiley, 2013.

[3] J. G. Andrews, R. K. Ganti, M. Haenggi, N. Jindal, and S. Weber, "A primer on spatial modeling and analysis in wireless networks," IEEE Communications Magazine, vol. 48, no. 11, pp. 156–163, 2010.

[4] H. ElSawy, E. Hossain and M. Haenggi, "Stochastic Geometry for Modeling, Analysis, and Design of Multi-Tier and Cognitive Cellular Wireless Networks: A Survey," in Proc. IEEE Communications Surveys & Tutorials, vol. 15, no. 3, pp. 996–1019, 2013.

[5] R. K. Ganti and M. Haenggi, "Interference and Outage in Clustered Wireless Ad Hoc Networks," IEEE Transactions on Information Theory, vol. 55, no. 9, pp. 4067-4086, 2009.

[6] C.-H. Lee and M. Haenggi, "Interference and outage in poisson cognitive networks," IEEE Transactions on Wireless Communications, vol. 11, no. 4, pp. 1392–1401, 2012.

[7] C. Saha, and H. S. Dhillon, and N. Miyoshi, and J. G. Andrews, "Unified analysis of HetNets using Poisson cluster processes under max-power association," IEEE Transactions on Wireless Communications, vol. 18, no. 8, pp. 3797–3812, 2019.

[8] B. Romanous, N. Bitar, A. Imran, and H. Refai, "Network densification: Challenges and opportunities in enabling 5G," in Proc. 2015 IEEE 20th International Workshop on Computer Aided Modelling and Design of Communication Links and Networks (CAMAD), pp. 129–134, 2015.

[9] R. Arshad, H. Elsawy, S. Sorour, T. Y. Al-Naffouri, and M.-S. Alouini, "Handover management in dense cellular networks: A stochastic geometry approach," in Proc. 2016 IEEE International Conference on Communications (ICC), pp. 1-7, 2016.

[10] ——, "Velocity-aware handover management in two-tier cellular networks," IEEE Transactions on Wireless Communications, vol. 16, pp. 1851–1867, 2017.

[11] ——, "Cooperative handover management in dense cellular networks," in Proc. 2016 IEEE Global Communications Conference (GLOBECOM), pp. 1–6, 2016.

[12] ——, "Handover management in 5G and beyond: A topology aware skipping approach," IEEE Access, vol. 4, pp. 9073–9081, 2016.

[13] E. Demarchou, C. Psomas, and I. Krikidis, "Mobility management in ultra-dense networks: Handover skipping techniques," IEEE Access, vol. 6, pp. 11921–11930, 2018.

[14] C. Suarez-Rodriguez, Y. He, B. A. Jayawickrama and E. Dutkiewicz, "Low-overhead handover-skipping technique for 5G networks," in Proc. 2019 IEEE Wireless Communications and Networking Conference (WCNC), pp. 1-6, 2019.

[15] X. Wu, and H. Haas, "Handover skipping for LiFi," IEEE Access, vol. 7, pp. 38369–38378, 2019.

[16] K. Tokuyama and N. Miyoshi, "Data rate and handoff rate analysis for user mobility in cellular networks," in Proc. 2018 IEEE Wireless Communications and Networking Conference (WCNC), pp. 1-6, 2018.

[17] K. Tokuyama, T. Kimura and N. Miyoshi, "Periodic Handover Skipping in Cellular Networks: Spatially Stochastic Modeling and Analysis," IEEE Transactions on Wireless Communications, doi: 10.1109/TWC.2023.3275926, 2023.

[18] Y. Xu, K. Tokuyama, and Y. Wada, "Handover skipping analysis in dense cellular network using Poisson cluster process," in Proc. 2022 IEEE 95th Vehicular Technology Conference (VTC2022-Spring), 2022.

[19] J. G. Andrews, F. Baccelli and R. K. Ganti, "A Tractable Approach to Coverage and Rate in Cellular Networks," IEEE Transactions on Communications, vol. 59, no. 11, pp. 3122–3134, 2011.

[20] H. S. Dhillon, R. K. Ganti, F. Baccelli, and J. G. Andrews, "Modeling and analysis of K-tier downlink heterogeneous cellular networks," IEEE Journal on Selected Areas in Communications, vol. 30, pp. 550–560, 2012.

[21] M. Di Renzo, A. Guidotti, and G. E. Corazza, "Average rate of downlink heterogeneous cellular networks over generalized fading channels: A stochastic geometry approach," IEEE Transactions on Communications, vol. 61, pp. 3050–3071, 2013.

[22] F. Baccelli and S. Zuyev, "Stochastic geometry models of mobile communication networks," Frontiers in Queueing: Models and Applications in Science and Engineering, J. H. Dshalalow, Ed. Boca Raton: CRC Press, 1997, ch. 8, pp. 227–243.

[23] X. Lin, R. K. Ganti, P. J. Fleming, and J. G. Andrews, "Towards understanding the fundamentals of mobility in cellular networks," IEEE Transactions on Wireless Communications, vol. 12, pp. 1686–1698, 2013.

[24] W. Bao and B. Liang, "Stochastic Geometric Analysis of User Mobility in Heterogeneous Wireless Networks," IEEE Journal on Selected Areas in Communications, vol. 33, no. 10, pp. 2212-2225, 2015.

[25] M. Tayyab, X. Gelabert, R. Jantti, "A survey on handover management: From LTE to NR," IEEE Access, vol. 7, pp. 118907–118930, 2019.

[26] A. H. Zahran, B. Liang, and A. Saleh, "Signal threshold adaptation for vertical handover in heterogeneous wireless networks," Mobile Networks and Applications, vol. 11, pp. 625–640, 2006.

[27] H. Zhang, W. Ma, W. Li, W. Zheng, X. Wen, and C. Jiang, "Signalling cost evaluation of handover management schemes in LTE-advanced femtocell," in Proc. 2011 IEEE 73rd Vehicular Technology Conference (VTC2011-Spring), pp. 1–5, 2011.

[28] M. Ylianttila, M. Pande, J. Makela and P. Mahonen, "Optimization scheme for mobile users performing vertical hand-offs between IEEE 802.11 and GPRS/EDGE networks," in Proc. 2001 IEEE Global Communications Conference (GLOBECOM), vol. 6, pp. 3439–3443, 2001.

[29] W. Bao and B. Liang, "Stochastic geometric analysis of handoffs in user-centric cooperative wireless networks," in Proc. IEEE INFOCOM2016 —The 35th Annual IEEE International Conference on Computer Communications, 2016.

[30] A. Chattopadhyay, B. Błaszczyszyn, and E. Altman, "Two-tier cellular networks for throughput maximization of static and mobile users," IEEE Transactions on Wireless Communications, vol. 18, no. 2, pp. 997–1010, 2019.

[31] S. Sadr and R. S. Adve, "Handoff Rate and Coverage Analysis in Multi-Tier Heterogeneous Networks," IEEE Transactions on Wireless Communications, vol. 14, no. 5, pp. 2626–2638, 2015.

[32] N. Bhushan, J. Li, D. Malladi, R. Gilmore, D. Brenner, A. Damnjanovic, R. T. Sukhavasi, C. Patel, and S. Geirhofer, "Network densification: The dominant theme for wireless evolution into 5G," IEEE Communications Magazine, vol. 52, no. 2, pp. 82—89, 2014.

[33] M. Kamel, W. Hamouda, and A. Youssef, "Ultra-dense networks: A survey," IEEE Communications Surveys & Tutorials, vol. 18, no. 4, pp. 2522—2545, 2016.

[34] H. ElSawy, A. Sultan-Salem, M.-S. Alouini, and M. Z. Win, "Modeling and analysis of cellular networks using stochastic geometry: A tutorial," IEEE Communications Surveys & Tutorials, vol. 19, no. 1, pp. 167–203, 2017.

[35] H. Tabassum, M. Salehi, and E. Hossain, "Fundamentals of mobility-aware performance characterization of cellular networks: A tutorial," IEEE Communications Surveys & Tutorials, vol. 21, no. 3, pp. 2288–2308, 2019.

[36] F. Baccelli, M. Klein, M. Lebourges, and S. Zuyev, "Stochastic geometry and architecture of communication networks," Telecommunications Systems, vol. 7, no. 1–3, pp. 209–227, 1997.

[37] Y. Hong, X. Xu, M. Tao, J. Li, and T. Svensson, "Cross-tier handover analyses in small cell networks: A stochastic geometry approach," in Proc. 2015 IEEE International Conference on Communications (ICC), pp. 3429–3434, 2015.

[38] B. Błaszczyszyn, M. Haenggi, P. Keeler, and S. Mukherjee, *Stochastic Geometry Analysis of Cellular Networks*. Cambridge: Cambridge University Press, 2018.

[39] 3GPP, "Evolved universal terrestrial radio access (E-UTRA); radio resource control (RRC); protocol specification," 3rd Generation Partnership Project (3GPP), Technical Specification (TS) 36.331, March 2020, v16.0.0.

[40] H. Q. Nguyen, F. Baccelli, and D. Kofman, "A stochastic geometry analysis of dense IEEE 802.11 networks," in Proc. IEEE INFOCOM 2007 —26th IEEE International Conference on Computer Communications, pp. 1199–1207 2007.

[41] J. Møller, "Random tessellations in $\mathbb{R}^d$," Advances in Applied Probability, vol. 21, no. 1, pp. 37–73, 1989.

[42] F. Baccelli and S. Zuyev, "Poisson-voronoi spanning trees with applications to the optimization of communication networks," Operations Research, vol. 47, no. 4, pp. 619–631, 1999.

[43] K. A. Hamdi, "A useful lemma for capacity analysis of fading interference channels," IEEE Transactions on Communications, vol. 58, no. 2, pp. 411–416, 2010.

[44] D. J. Daley and D. Vere-Jones, *An Introduction to the Theory of Point Processes: Volume II: General Theory and Structure*, 2nd ed. Springer, 2008.

[45] A. J. Fehske, I. Viering, J. Voigt, C. Sartori, S. Redana and G. P. Fettweis, "Small-Cell Self-Organizing Wireless Networks," in Proc. IEEE, vol. 102, no. 3, pp. 334-350, 2014.

[46] G. Wang, Y. Zhong, R. Li, X. Ge, T. Q. S. Quek and G. Mao, "Effect of Spatial and Temporal Traffic Statistics on the Performance of Wireless Networks," IEEE Transactions on Communications," vol. 68, no. 11, pp. 7083-7097, 2020.

[47] C. Saha, M. Afshang and H. S. Dhillon, "3GPP-Inspired HetNet Model Using Poisson Cluster Process: Sum-Product Functionals and Downlink Coverage," IEEE Transactions on Communications, vol. 66, no. 5, pp. 2219-2234, 2018.

[48] W. Bao and B. Liang, "Handoff rate analysis in heterogeneous wireless networks with Poisson and Poisson cluster patterns," in Proc. the 16th ACM International Symposium on Mobile Ad Hoc Networking and Computing pp. 77–86, 2015.

[49] H. Zhou, H. Zhou, J. Li, K. Yang, J. An and X. Shen, "Heterogeneous Ultradense Networks With Traffic Hotspots: A Unified Handover Analysis," IEEE Internet of Things Journal, vol. 10, no. 10, pp. 8825–8838, 2023.

[50] N. M. Kibinda and X. Ge, "User-Centric Cooperative Transmissions-Enabled Handover for Ultra-Dense Networks," IEEE Transactions on Vehicular Technology, vol. 71, no. 4, pp. 4184–4197, 2022.

[51] H. Ishii, Y. Kishiyama, and H. Takahashi, "A novel architecture for LTE-B :C-plane/U-plane split and phantom cell concept," in Proc. IEEE Globecom Workshops, pp. 624–630, 2012.

[52] H. Ibrahim, H. ElSawy, U. T. Nguyen and M. -S. Alouini, "Mobility-Aware Modeling and Analysis of Dense Cellular Networks With C -Plane/ U -Plane Split Architecture," in IEEE Transactions on Communications, vol. 64, no. 11, pp. 4879–4894, 2016.

[53] B. Soret, A. D. Domenico, S. Bazzi, N. H. Mahmood and K. I. Pedersen, "Interference Coordination for 5G New Radio," in IEEE Wireless Communications," vol. 25, no. 3, pp. 131–137, 2018.

[54] R. Arshad, L. Lampe, H. ElSawy and M. J. Hossain, "Integrating UAVs into Existing Wireless Networks: A Stochastic Geometry Approach," 2018 IEEE Globecom Workshops (GC Wkshps), pp. 1–6, 2018.

[55] S. S. Kalamkar, F. Baccelli, F. M. Abinader, A. S. M. Fani and L. G. U. Garcia, "Beam Management in 5G: A Stochastic Geometry Analysis," in IEEE Transactions on Wireless Communications, vol. 21, no. 4, pp. 2275–2290, 2022.